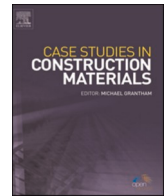




ELSEVIER

Contents lists available at [ScienceDirect](https://www.sciencedirect.com)

Case Studies in Construction Materials

journal homepage: www.elsevier.com/locate/cscm

Self-compacting concrete with recycled concrete aggregate subjected to alternating-sign temperature variations: Thermal strain and damage

Víctor Revilla-Cuesta^{a,*}, Marta Skaf^b, Amaia Santamaría^c, Ana B. Espinosa^b,
Vanessa Ortega-López^a

^a Department of Civil Engineering, Escuela Politécnica Superior, University of Burgos, c/ Villadiego s/n, 09001 Burgos, Spain

^b Department of Construction, Escuela Politécnica Superior, University of Burgos, c/ Villadiego s/n, 09001 Burgos, Spain

^c Department of Mechanical Engineering, Escuela de Ingeniería de Bilbao I, University of the Basque Country, Pl. Ingeniero Torres Quevedo 1, 48013 Bilbao, Spain

ARTICLE INFO

Keywords:

Self-compacting concrete
Recycled concrete aggregate
Extreme-ambient cyclical temperature increases
Linear thermal expansion coefficient
Internal damage
Hygroscopicity

ABSTRACT

Any variation in temperature alters the dimensions of a concrete structure and provokes thermal stress. Moreover, the propagation of micro-cracking decreases the strength of concrete that is exposed to sub-zero temperatures (freezing), to heat phenomena (heating), or to cyclical thermal variations, especially when prepared using Recycled Concrete Aggregate (RCA). A reference self-compacting concrete (SCC) mix made with 100% coarse and fine natural aggregate and three SCC mixes containing 100% coarse and/or fine RCA in replacement of natural aggregate were tested in this study of the thermal performance of SCC and the related effects of RCA. The mixtures were subjected to five thermal tests designed with positive and negative, and both constant and cyclical, extreme-ambient temperature variations, reaching temperatures of $-15\text{ }^{\circ}\text{C}$ and $70\text{ }^{\circ}\text{C}$. Stiffness, weight, compressive strength, thermal deformability, and internal damage of the SCC mixtures were monitored throughout suitable testing. Internal damage, hygroscopicity, and loss of strength increased at temperatures below $0\text{ }^{\circ}\text{C}$, especially in the mixtures containing 100% coarse RCA, although the SCC manufactured with simultaneous additions of fine and coarse RCA fractions showed the worst performance. Overall, RCA performed better under positive temperature variations. The test results lead to the recommendation of a linear thermal expansion coefficient of $1.2 \cdot 10^{-5}\text{ }^{\circ}\text{C}^{-1}$ in calculations for SCC containing RCA under those extreme environmental conditions.

1. Introduction

Concrete consists of binder, aggregates, setting catalyzers (water, reagents) and, optionally, admixtures and/or additions [1,2]. It has two separate states, as its viscous consistency in the fresh state is quite unlike its robust solidity in the hardened state [3,4]. Despite its sound appearance, temperature variations within a certain range of environmental conditions will affect its strength and deformational behavior [5] in three different ways. Firstly, its strength will depend on the curing temperature [6]. High temperatures favor

* Corresponding author.

E-mail address: vrevilla@ubu.es (V. Revilla-Cuesta).

<https://doi.org/10.1016/j.cscm.2022.e01204>

Received 18 March 2022; Received in revised form 13 May 2022; Accepted 28 May 2022

Available online 30 May 2022

2214-5095/© 2022 The Author(s). Published by Elsevier Ltd. This is an open access article under the CC BY-NC-ND license (<http://creativecommons.org/licenses/by-nc-nd/4.0/>).

water evaporation and poor cement hydration, which will reduce final concrete strength, even though it accelerates the setting process [7]. Secondly, temperature variations produce internal damage within the concrete [5], by causing micro-cracks and slight chemical alterations in the capillary network and the Interfacial Transition Zones (ITZ) [8]. If negative (below 0 °C) temperatures are cyclically applied, this micro-cracking will quickly propagate, due to the volumetric change of capillary water within the concrete when it freezes [9]. Finally, any temperature variation will alter the dimensions of concrete structures, since concrete will contract when the temperature decreases and will expand when the temperature variation is positive [10]. This deformation causes macroscopic stresses and cracks within all types of structures, from beams [11] to dams [12], that must be considered in their design [13].

The thermal response of concrete is occasionally affected by changes in its composition. On the one hand, it is slightly different for each type of concrete [14], because of the different proportion of their components [15]. For example, Self-Compacting Concrete (SCC), characterized by its high flowability [16], appears to have a higher thermal deformability than a vibrated one [17]. Furthermore, the use of Natural Aggregates (NA) [18] or binders [19] of different nature, the addition of fibers [20], or even the use of by-products to replace conventional materials [21] can modify the thermal conductivity of a concrete [22], its thermal deformability [10], and its deterioration, due to the micro-cracking discussed in the previous paragraph [8]. As the effect of each by-product differs [22], this paper is focused on analyzing the behavior of concrete produced with Recycled Concrete Aggregate (RCA).

Perhaps, RCA is the most widely used by-product in concrete production due to its abundance and low cost [23,24], as well as its good properties when the residue consists of crushed precast concrete elements [25]. Its defining characteristic is its high water absorption, due to the adhered mortar of the coarser particles [26], and crushed mortar particles on the finest fractions [27]. RCA can successfully replace NA, if the composition of the concrete retains its singular properties [28]. On the one hand, the water content of the mix must be increased when RCA is added, to balance its high water absorption levels, in order to ensure concrete workability [29], especially in SCC [30]. On the other hand, the use of any RCA fraction increases the porosity of the mixture, which is also negative in view of its durability behavior [31]. Moreover, the RCA content added to concrete mixes must be carefully defined, as it decreases concrete strength [32], commonly due to the lower quality ITZs produced by RCA [33], and the presence of contaminants and altered mortar in the fine fraction [34]. However, the use of coarse RCA without any treatment can lead to an improvement of the mechanical behavior of the concrete, due to the characteristic features forming the ITZs. On the one hand, if coarse RCA of adequate quality is used and the mix design is properly adjusted, the ITZs are enhanced, and the strength of the concrete can be increased up to 50% coarse RCA [26,32]. On the other hand, the ITZs formed by using RCA have a lower energy-dissipation capacity, which improves the high-strain rate compressive behavior of concrete [35]. Furthermore, RCA treatment improves its performance. For example, a slightly expensive though useful alternative is to subject this by-product to high temperatures of around 650–800 °C prior to its use, which will considerably reduce the amount of adhered mortar [36], and will improve the shape of RCA, as some models for predicting the mechanical behavior of concrete with RCA show that the variation in mechanical properties caused by a certain percentage of coarse RCA is directly related to the geometric index of this alternative aggregate [37]. Another alternative is to subject RCA to carbonation treatments, which strengthens the adhered mortar [38].

The thermal behavior of concrete manufactured with RCA has been analyzed at extremely high (burning) temperatures, so the use of coarse RCA favors the micro-cracking of concrete at temperatures higher than 400 °C [39]. If concrete is exposed to such temperatures, this aggregate notably decreases concrete strength [40,41], decreases any plastic strain [42,43], and increases the sensitivity of concrete to lateral stress, leading to a higher increase of compressive strength under lateral confinement [44]. Furthermore, a high content of impurities in RCA can accelerate the damage of concrete following a heating process [21]. Coarse RCA also affects the thermal deformability of concrete [17], increasing it in pumpable concrete [45], and decreasing it in paving concrete [10], which shows that the effect of RCA on the linear thermal expansion coefficient seems to be linked to mix workability. The use of coarse RCA also reduces the thermal conductivity of concrete [46], which is useful for improved thermal behavior in, for example, façade components [47].

From the discussion in this introduction and the accompanying references, it may be noted that several relevant aspects related to the thermal behavior of RCA concrete have yet to be evaluated, such as:

- The strength behavior of SCC with RCA when it reaches temperatures below 0 °C.
- The deformational behavior of SCC under both positive and negative and constant and cyclical temperature variations.
- The effect of fine RCA and its use in SCC on thermal performance, related to its strength, stiffness, and thermal deformability.

The aim of this study is to address all the above points, for which purpose it analyzes the thermal behavior of four SCC mixes of slump flow from 750 to 850 mm, slump-flow class SF3 as per EFNARC [48], manufactured using 100% coarse and/or fine RCA. SCC mixtures were tested under five different thermal conditions, consisting of both positive and negative and both constant and cyclical temperature variations. The evolution of their thermal deformability and, therefore, of their linear thermal expansion coefficient throughout all the tests was monitored. In addition, the internal damage (micro-cracking) and the compressive strength losses of each mix were evaluated after each test. Finally, the hygroscopicity of each mix was also analyzed. The intention behind this study is to expand on the results presented in a previous letter by the authors [17], some of which are repeated in this paper to offer a complete view of the thermal behavior of SCC manufactured with both RCA fractions.

2. Materials and methods

2.1. Raw materials

The four SCC mixes produced in this study consisted of CEM I 52.5 R (EN 197-1 [49]), with a density of 3.1 Mg/m^3 , water, a viscosity regulator for high flowability and self-compactability, and a plasticizer to reduce the amount of water required to reach an SF3 slump-flow class (EFNARC [48]) in the mixtures. In addition, three different types of aggregates were used, whose granulometry and physical properties are shown in Fig. 1 and Table 1, respectively:

- The high content of fines needed to obtain SCC [15] was reached by adding suitably ground limestone (fines 0/1 mm). This aggregate, commonly used to produce mortars, had a high volume of particles lower than 0.063 mm (see Fig. 1).
- The control concrete was produced with both siliceous sand 0/4 mm and siliceous gravel 4/12.5 mm. These aggregates were characterized by their rounded shapes. In addition, the low content of fine particles in the siliceous sand from the region (see Fig. 1) was compensated by the above-mentioned limestone fines 0/1 mm.
- The three RCA mixtures were manufactured by replacing 100% fine and/or coarse NA with this by-product. The RCA was supplied from a local waste treatment company within a size range of 0/31.5 mm. RCA was manufactured from crushed precast concrete elements with a compressive strength greater than 50 MPa that had been rejected due to aesthetic and/or geometric defects. As the size of the RCA was not suitable to produce SCC, it was sieved in the laboratory to obtain two fractions, 4/12.5 mm and 0/4 mm, thereby assimilating this aggregate to the siliceous NA in use. RCA was less dense than NA, although its water absorption was 2–3 times higher (see Table 1). The chemical composition of RCA is shown in Table 2.

2.2. Mix designs

As stated above, four mixtures were performed. Firstly, a control concrete was produced, labeled SCC0/0, that contained 100% coarse (4/12.5 mm) and fine (0/4 mm) siliceous NA and a suitable amount of limestone fines 0/1 mm. The proportions of its different components, shown in Table 3, were determined according to the requirements of Eurocode 2 [13]. An optimal adjustment to the Fuller curve was established for a particle content lower than 0.250 mm (see Fig. 2). Moreover, a water-to-cement (w/c) ratio of 0.55 was defined for the mix (effective w/c ratio of 0.50), as in other similar studies [16]. These last two aspects and the suitable use of admixtures yielded an SCC of slump-flow class SF3 [48].

Subsequently, three mixtures were produced by replacing 100% coarse and/or fine NA with RCA, retaining a constant amount of limestone fines (0/1 mm). The NA replacement was performed for each whole fraction (4/12.5 mm and/or 0/4 mm) by volume; no size-by-size replacement was performed, using the most economic and widespread procedure in the recycled-concrete industry [50]. Nevertheless, this procedure slightly increased the fines content in the mixes manufactured with fine RCA, as shown in Fig. 2. The mixes were labeled SCC100/0 (100% coarse RCA instead of coarse NA), SCC0/100 (100% fine RCA instead of fine NA), and SCC100/100 (100% coarse and fine RCA instead of both NA fractions).

The notable water absorption of RCA reduces the effective w/c ratio and, in turn, concrete workability, if the volume of mix water remains unchanged when NA is replaced by RCA [29]. In this study, the mixtures had to share a very similar flowability in order to compare the results of the different SCC mixes in terms of their performance [32]. In this way, the flowability target of all the mixes was a slump-flow class SF3 [48]. The water content was therefore increased when RCA was added. In mixtures SCC0/0, SCC100/0, and SCC0/100, the effective w/c ratio was held constant, equal to 0.50 units as shown in Table 3, since in all cases the desired slump-flow class was achieved. The flowability of mixture SCC100/100 was negatively affected by both the surface roughness of coarse and fine

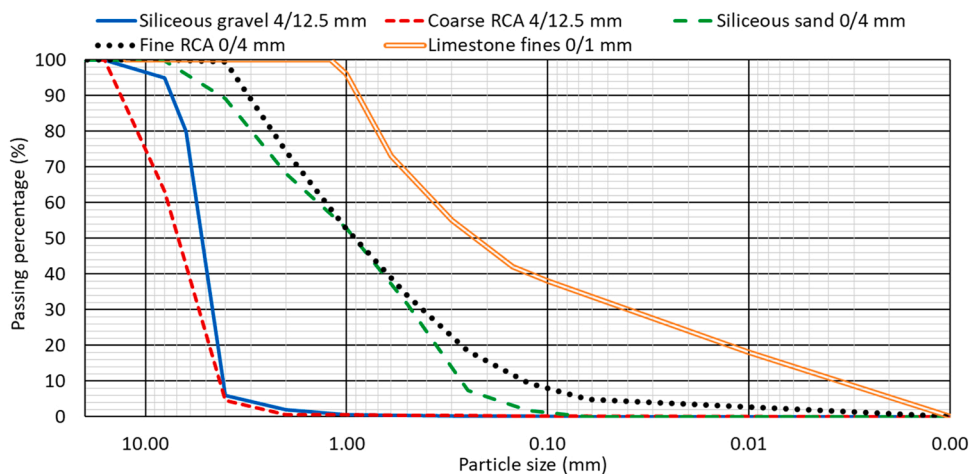


Table 1

Physical properties of the aggregates.

Aggregate	Saturated-surface-dry density (Mg/m ³), EN 1097-6[49]	24-h water absorption (%), EN 1097-6[49]	10-minute water absorption (%)	Fineness modulus
Limestone fines 0/1 mm	2.61	2.53	1.89	1.30
Fine NA 0/4 mm	2.57	0.25	0.18	3.49
Fine RCA 0/4 mm	2.38	7.36	6.03	3.12
Coarse NA 4/12.5 mm	2.61	0.84	0.66	5.27
Coarse RCA 4/12.5 mm	2.43	6.25	5.28	6.30

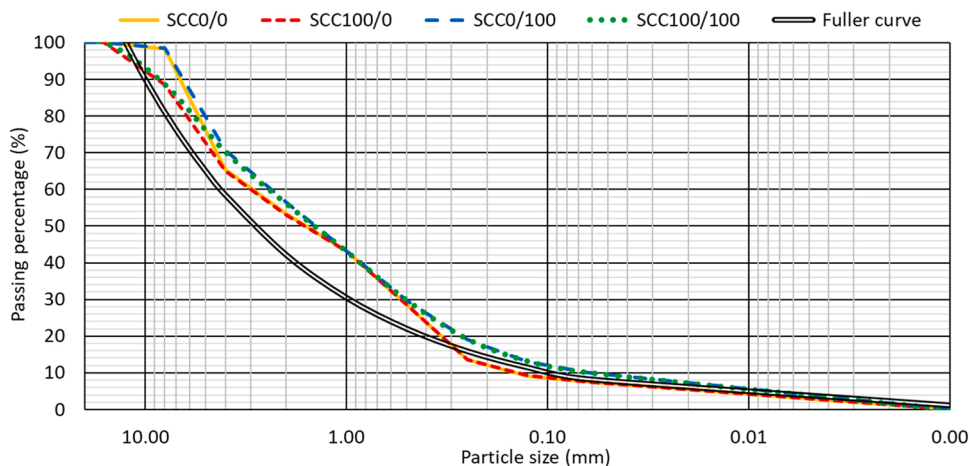
Table 2

Chemical composition of RCA 0/4 mm (% in weight) obtained through X-ray fluorescence.

SiO ₂	CaO	Al ₂ O ₃	Fe ₂ O ₃	SO ₃	MgO	K ₂ O	TiO ₂	P ₂ O ₅	Others (CO ₂ ...)
50.80	20.00	3.74	1.12	1.00	0.63	0.60	0.15	0.06	21.9

Table 3Mix design (kg/m³).

Aggregate	SCC0/0	SCC100/0	SCC0/100	SCC100/100
Cement	300	300	300	300
Water	165	190	230	285
Viscosity regulator	2.20	2.20	2.20	2.20
Plasticizer	4.50	4.50	4.50	4.50
Limestone fines 0/1 mm	340	340	340	340
Fine NA 0/4 mm	940	940	0	0
Fine RCA 0/4 mm	0	0	865	865
Coarse NA 4/12.5 mm	575	0	575	0
Coarse RCA 4/12.5 mm	0	530	0	530
Effective w/c ratio	0.50	0.50	0.50	0.60

**Fig. 2.** Global granulometry of the mixes.

RCA [30] and the fast mixing process that was conducted (see Section 2.3), with which the water absorption of the aggregates was not maximized [50]. Hence, the effective w/c ratio in mixture SCC100/100 had to be increased to a value of 0.60 units (Table 3) to reach the slump-flow target. The content of the two admixtures was not modified to prevent their segregation after mixing.

2.3. Experimental program

The mixing process had only one stage. Firstly, all the aggregates, cement, and half of the water were placed in the concrete mixer.

Then, the mixer was turned on and the remaining water was added continuously for 30 s while mixing continued. Subsequently, the admixtures were poured into the mixer and mixing continued for a further 30 s. As mentioned above, the mixtures with only one RCA fraction (coarse or fine) showed good fresh behavior; however, the effective w/c ratio of mix SCC100/100 had to be increased.

After mixing, the slump-flow test (EN 12350-8 [49]) was carried out at 0 and 30 min. In addition, different specimens were manufactured to perform the hardened-state tests. The specimens were kept in a moist room (temperature of $20 \pm 2 \text{ }^\circ\text{C}$ and humidity $95 \pm 5\%$) until the test. The following specimens were manufactured for each mixture:

- Eight 10×20 -cm cylindrical specimens to determine the mechanical properties: compressive strength (EN 12390-3 [49]) and modulus of elasticity (EN 12390-13 [49]) at 7 and 28 days. Two samples were used in each test at each age.
- Eleven $75 \times 75 \times 275$ -mm prismatic specimens to perform the thermal tests. This specimen size was chosen because it had suitable dimensions for easy handling when moved in and out of the freezer and oven during thermal testing. In addition, thermal strain could be easily measured on its prismatic shape, similar to the concrete components most commonly exposed to thermal variations such as beams and columns [42]. All these specimens were placed in the moist room over 24 h until demolding, and then exposed to the laboratory environment over 180 days, thereby assuring their dimensional stabilization after the period of concrete drying shrinkage [26]. Two specimens were used for each of the five thermal tests, and the remaining specimen, also exposed to the laboratory environment, was used to measure the reference compressive strength (see Section 3.5).

2.3.1. Thermal tests

The main novelty of this research work refers to the thermal tests, which were designed by the authors of this article, due to a lack of standards and recommendations for their implementation. These tests were used to analyze novel aspects related to the thermal behavior of RCA concrete, such as deformability, internal damage, and hygroscopicity.

Three different temperatures were firstly defined in order to perform these tests. Each one simulated extreme, yet commonplace, thermal conditions to which a concrete structure can be exposed. The temperature values for the thermal tests were defined according to the common temperatures reached in the freeze/thaw (temperature variation between $-15 \text{ }^\circ\text{C}$ and $20 \text{ }^\circ\text{C}$) and moist/dry (temperature variation between $20 \text{ }^\circ\text{C}$ and $70 \text{ }^\circ\text{C}$) tests [9]:

- Ambient temperature: $20 \pm 1 \text{ }^\circ\text{C}$. A climatic chamber with this temperature and humidity $60 \pm 5\%$, both automatically controlled, was used to obtain this temperature without fluctuations.
- Minimum temperature: $-15 \pm 1 \text{ }^\circ\text{C}$. The samples were subjected to this temperature in a freezer.
- Maximum temperature: $70 \pm 1 \text{ }^\circ\text{C}$. The temperature to which the specimens were subjected in an oven.

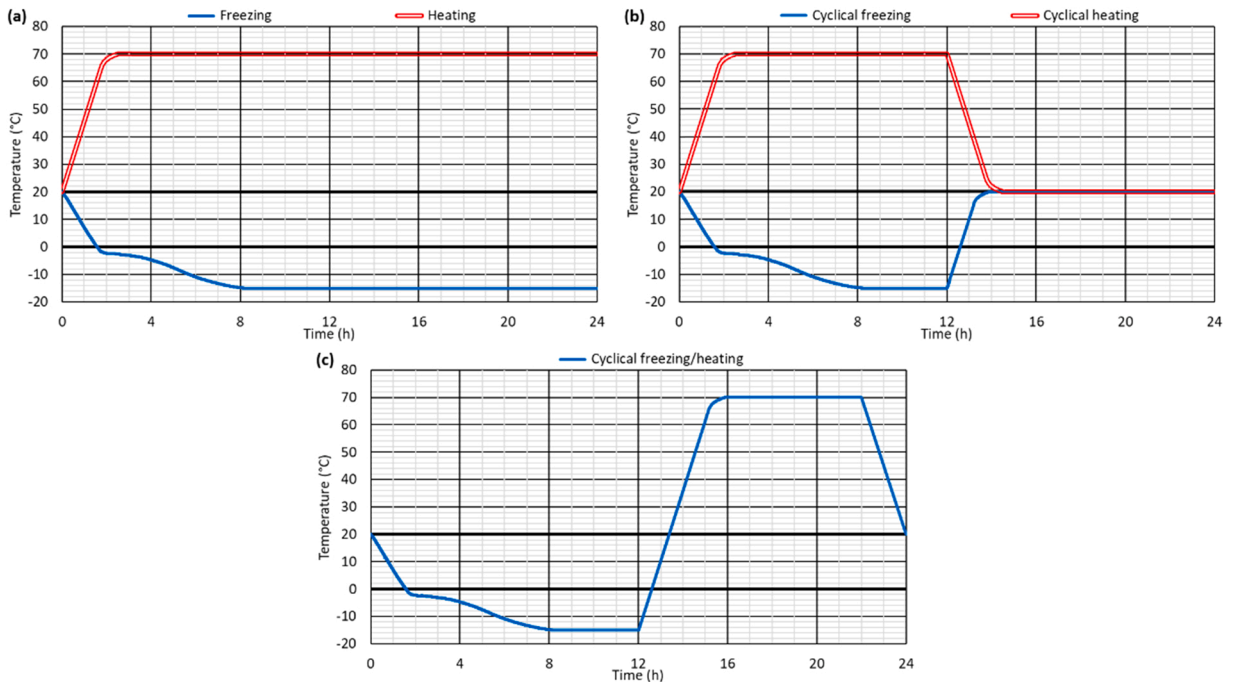


Fig. 3. Temperature evolution during the first 24 h of (a) freezing and heating tests; (b) cyclical-freezing and cyclical-heating tests; (c) cyclical-freezing/heating test.

Subsequently, the average duration of day and night time in the northern hemisphere was estimated following a brief bibliographical review [51–53]. In this review, the average exposure times of a concrete structure to certain temperatures were estimated. Finally, average times of 12 h were chosen for both daytime and nighttime duration. It was therefore decided that when applying cyclical temperature variations, the exposure time of the specimens to each temperature should be 12 h.

From these three temperatures and a duration of the cycles of 12 h, five thermal tests were designed. A freezing test and a heating test were defined to study the behavior of the mixtures when the specimens were continuously subjected to a nominal temperature (constant-temperature tests). The behavior of the mixtures under cyclical temperature variations, an aspect that must always be considered in the design of concrete structures [13], could be analyzed from the results of the other three tests (cyclical-temperature tests). The duration of the constant-temperature tests (168 h) and the number of cycles in the cyclical-temperature tests (20 cycles) were fixed, bearing in mind that the objective was to simulate extreme service conditions of concrete, not to cause its failure [54]. Accordingly, the following thermal tests were conducted:

- Freezing test. The specimens were held at a temperature of $-15\text{ }^{\circ}\text{C}$ (in a freezer) for 168 h (1 week).
- Heating test. The specimens were kept at a temperature of $70\text{ }^{\circ}\text{C}$ (in an oven) for 168 h (1 week).
- Cyclical-freezing test. The specimens were exposed to 20 cycles consisting of 12 h at $-15\text{ }^{\circ}\text{C}$ (freezer) and 12 h at ambient temperature (climatic room).
- Cyclical-heating test. The samples were exposed to 20 cycles consisting of 12 h at $70\text{ }^{\circ}\text{C}$ (oven) and 12 h at ambient temperature (climatic room).
- Cyclical-freezing/heating test. The prismatic samples were exposed to 20 cycles consisting of 12 h at $-15\text{ }^{\circ}\text{C}$ (freezer) and 12 h at $70\text{ }^{\circ}\text{C}$ (oven).

The temperature trends throughout the first 24 h of each test were measured with a temperature probe inserted into the center of a specimen. These trends are shown in Fig. 3 where the exposure time of the center of the specimen to the surrounding temperature was at least 4 h. It can also be noted from Fig. 3 that the temperature variation was $-12\text{ }^{\circ}\text{C/h}$ when the temperature was decreasing as with the concrete freeze/thaw test [9], while it was $25\text{ }^{\circ}\text{C/h}$ when the temperature increased, to reach a constant temperature within approximately the same time as for the freezing phase. These rates showed that increasing the temperature in concrete required less energy and time than decreasing it [8], due to the freezing of capillary water, evidenced by the almost-constant temperature steps of the graphics that were registered between two and four hours of cooling when the temperature fell below $0\text{ }^{\circ}\text{C}$.

During the performance of the tests, the concrete strain was continuously measured by strain gauges and recorded by a suitable system. The linear shape of the $75\times 75\times 275\text{-mm}$ prismatic specimens meant that the predominant strain was along a longitudinal axis on which the strain measurements were taken [17]. In addition, the weight variations, Ultrasonic Pulse Velocity (UPV) evolution, and compressive strength, before and after each test, were evaluated. Detailed explanations of all the measurement techniques are given in the sections where the test results are discussed.

Finally, it is important to note that the above-mentioned temperatures occurred within the concrete mass, at the core of the samples. Thus, both partial decomposition of primary ettringite at higher temperatures, and micro-cracking after the capillary water had frozen and therefore expanded at lower temperatures, might be expected.

3. Results and discussion

3.1. Slump flow

The higher water absorption of RCA than NA decreases concrete workability [29], although it can be compensated by increasing the amount of mix water when using this alternative aggregate [50]. Moreover, the water absorption of RCA can be maximized in a multi-stage mixing process for better conservation of workability over time [55]. However, a single-stage mixing process was

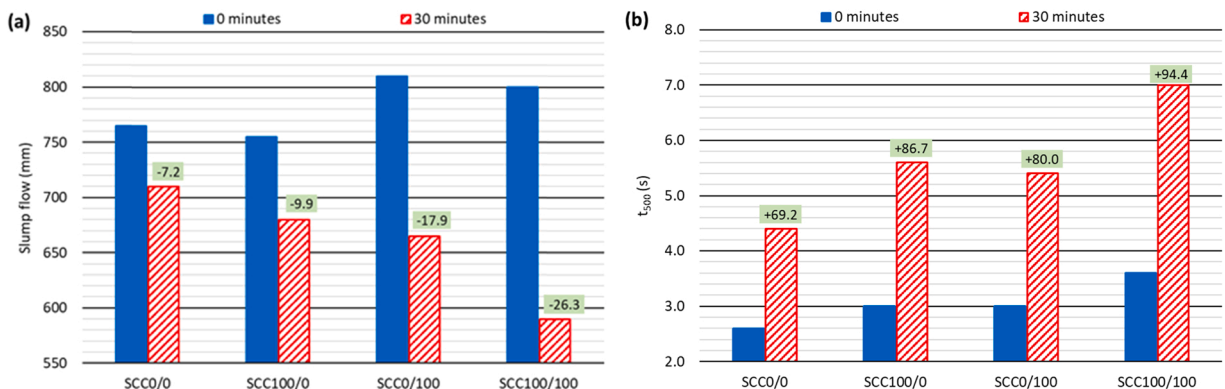


Fig. 4. Fresh behavior of the mixes: (a) slump flow; (b) viscosity t_{500} . The number is the variation from 0 to 30 min.

implemented in this study (see Sections 2.2 and 2.3). As shown in Fig. 4a, the mixtures with only one RCA fraction did achieve a slump-flow class SF3 with an effective w/c ratio of 0.50 through this mixing process, but the effective w/c ratio had to be increased to 0.60 in mixture SCC100/100 to obtain the same SF3 class. From the mixes with the same effective w/c ratio, it can be found that:

- The irregular shape and the higher fineness modulus of coarse RCA with respect to the NA slightly decreased the slump flow [29] (from 765 to 755 mm).
- The higher fines content of fine RCA 0/4 mm (fineness modulus of 3.12 units, Table 1), compared to siliceous sand 0/4 mm (fineness modulus of 3.49 units), increased the slump flow from 765 to 810 mm.
- The greater the total water absorption of the aggregate, the higher the temporal loss of flowability: 17.9% for mix SCC0/100 and 9.9% for mix SCC100/0.

On the other hand, as shown in Fig. 4b, the addition of any RCA fraction was slightly negative for SCC viscosity (t_{500}) due to the angular shape of RCA, which hindered its dragging by the cementitious matrix [56]. In this way, the addition of either coarse or fine RCA in mixtures with the same effective w/c ratio resulted in an increase in t_{500} from 2.6 to 3.0 s 30 min after the mixing process, all

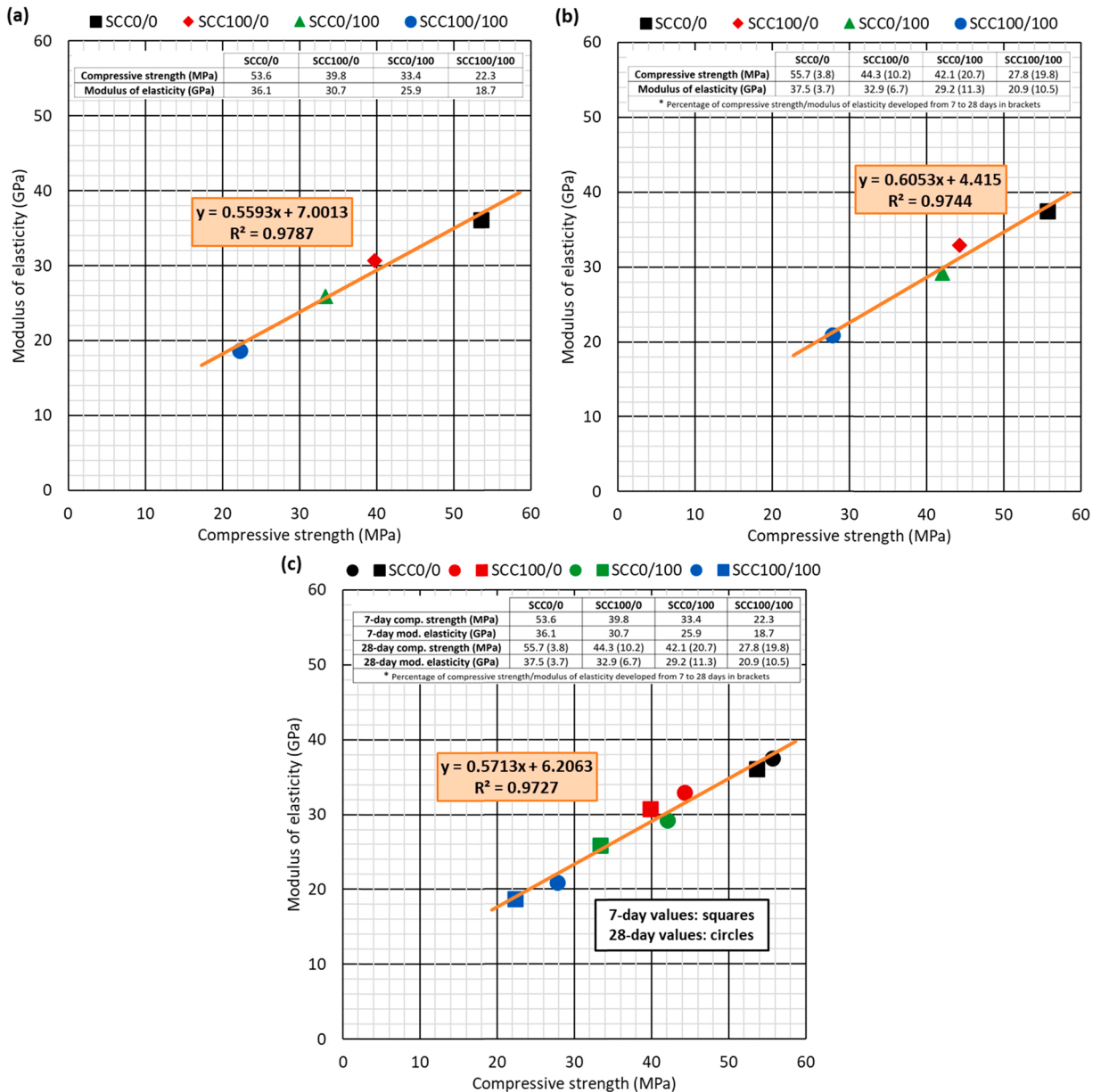


Fig. 5. Compressive strength and modulus of elasticity of the mixes: (a) 7 days; (b) 28 days; (c) both ages together.

SCC mixes with RCA experienced an increase in the t_{500} by around 80–90%, higher than that of mix SCC0/0.

3.2. Mechanical properties: compressive strength and modulus of elasticity

The compressive strength and modulus of elasticity of the mixes were measured at 7 and 28 days in specimens conserved in a moist room, which exhibited a clearly linear trend, with coefficients R^2 of around 97%, as shown in Fig. 5. Both properties increased with age, and decreased when adding any RCA fraction, although the use of fine RCA was more harmful than the addition of the coarse fraction of this waste [33]. So, the 28-day compressive strength and modulus of elasticity of the mix SCC100/0 were 44.3 MPa and 32.9 GPa, respectively, against 42.1 MPa and 29.2 GPa, respectively, for mixture SCC0/100. The joint use of both RCA fractions resulted in the largest decreases.

According to the available literature [32,34], the substitution of NA by RCA in the coarse fraction hardly affects the mechanical performance of SCC in mixes with a 100% fine RCA. However, in this research work, the performance of SCC0/100 (100% fine RCA) was substantially better than that of mixture SCC100/100 (100% coarse and fine RCA), due to two fundamental reasons:

- Firstly, the good quality of the fine fraction of the RCA, with a high SiO_2 and CaO content (see Table 2), factor also reported in other studies [57].
- Secondly, the higher effective w/c ratio of mixture SCC100/100, necessary to reach the required flowability with the single-stage mixing process, as discussed above.

RCA also delayed the evolution of the mechanical properties over time. In this way, the mechanical properties of the control mix SCC0/0 increased by only 4% from 7 to 28 days, while this increase was 7–10% for mix SCC100/0 and 11–20% for mixes SCC0/100 and SCC100/100. The higher temporal increases of the mechanical properties that incorporated fine RCA were because of the higher water absorption, which favored a more notable deferred hydration of cement [55].

3.3. Thermal deformability

3.3.1. Thermal strain

The longitudinal strain within the specimens was continuously measured by strain gauges during the five thermal tests that were performed. The gauges were arranged on three of the four longitudinal sides, as shown in Fig. 6. Data were collected and recorded at a frequency of 1 Hz and suitable temperature corrections were introduced according to the recommendations from the strain gauge manufacturer.

The strains obtained throughout the constant-temperature tests are shown in Fig. 7. In these tests, the different mixtures showed the expected general behavior. At first, the concrete experienced a very pronounced variation in strain, because the temperature varied very sharply until its stabilization (Fig. 3a). Subsequently, the temperature remained constant and, therefore, the strain as well. The results of these tests clearly revealed that the use of RCA increased the thermal deformability of SCC, maybe due to the higher flexibility, or perhaps higher dilatability, of this residue compared to NA [42].

- Under both positive and negative temperature increases, mixture SCC100/0 (100% coarse RCA) underwent greater strains than mixture SCC0/100 (100% fine RCA). The cementitious matrix of concrete adhered to RCA increased the flexibility/dilatability of this by-product compared to NA [42]. So, both mixtures SCC100/0 and SCC0/100 demonstrated greater deformability than the mixture manufactured with 100% NA. The minimum strains (at -15°C) in absolute value in the freezing test were 0.305 mm/m for mixture SCC100/0, 0.280 mm/m for mixture SCC0/100, and 0.250 mm/m for mixture SCC0/0. In the heating test, the maximum strains were 0.460 mm/m, 0.450 mm/m, and 0.385 mm/m, respectively. Since fine RCA only incorporates millimeter-sized mortar

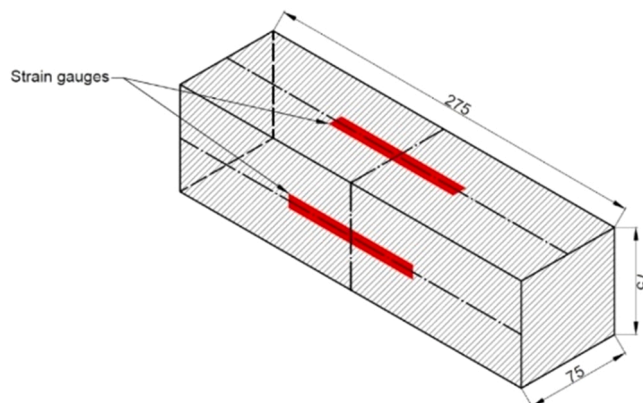


Fig. 6. Arrangement of strain gauges for strain measurement. Dimensions in mm.

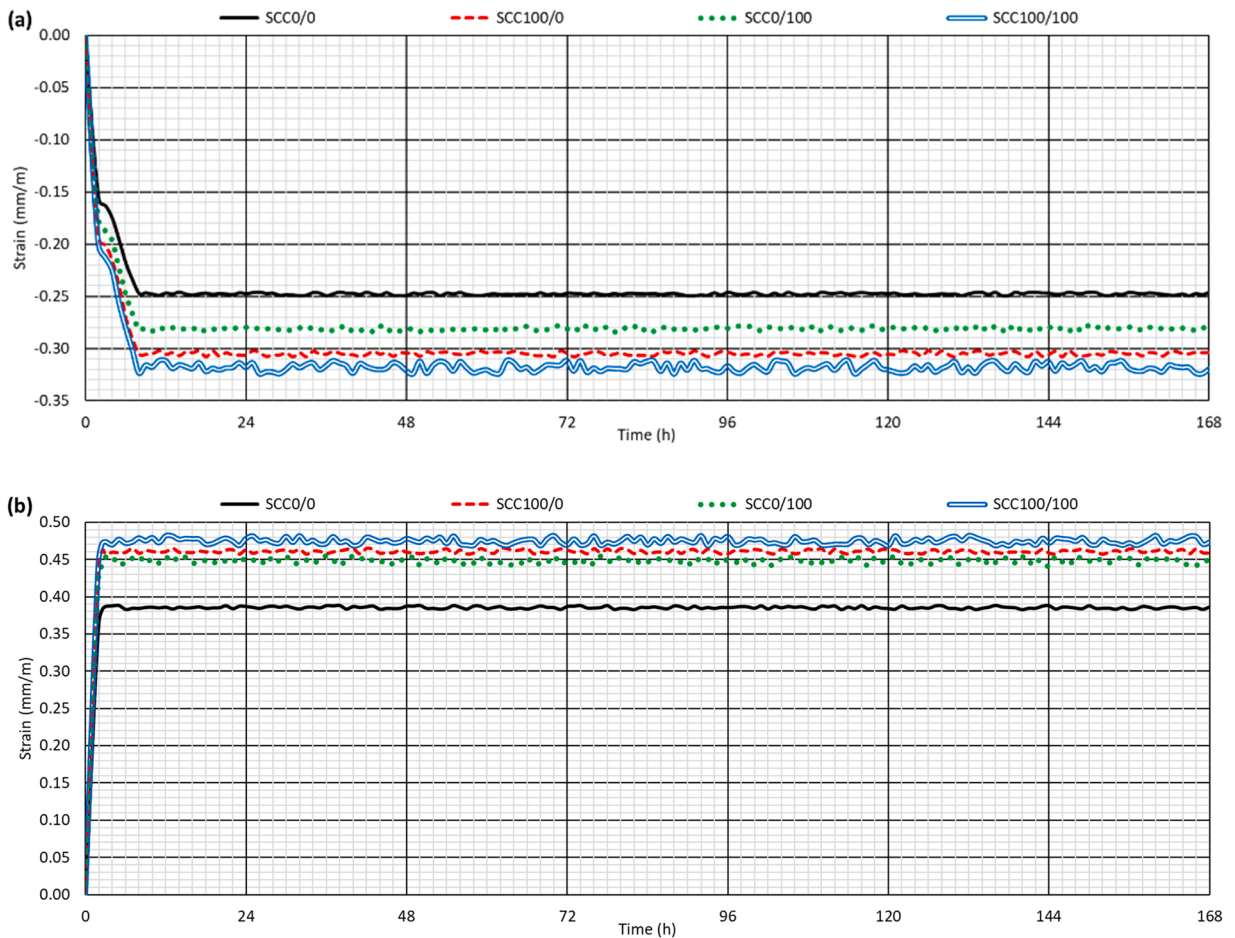


Fig. 7. Strain within mixtures during the (a) freezing test; (b) heating test.

particles [34], the presence of the old cementitious matrix as attached mortar rather than evenly-distributed particles favored the increase in global thermal deformability when adding coarse RCA [45].

- Mixture SCC100/100 showed slightly higher strains than mixture SCC100/0 in both tests, due to the joint effect of both RCA fractions. However, it had slightly higher strain fluctuations throughout the period of constant temperature. The increase in RCA content led to higher variability in concrete behavior [57] and, in consequence, thermal strain.
- The point at which the water froze, shown in Fig. 7a, during the initial cooling process shown in Fig. 3a, was evident due to the appearance of a step in the downward linear region of the curves.

The maximum and minimum strains that each mixture underwent in each cycle of the cyclical-temperature tests are shown in Fig. 8. These figures have previously been reported in another paper by the authors on cyclical-freezing and cyclical-heating tests [17]. These tests simulate the extreme, but possible, temperature variations that real concrete structures can undergo. Although the trends they showed were not as clear as the constant-temperature tests, in a similar way to the above-mentioned constant-temperature tests, they did show that mixture SCC100/0 (100% coarse RCA) underwent higher thermal strains than mixture SCC0/100, and that mixture SCC100/100 was the most deformable.

Moreover, during these tests, all the mixtures tended to shrink as the number of cycles increased. On the one hand, this phenomenon was observed in the progressive decrease of the maximum (at 70 °C) strain in both cyclical-heating and cyclical-freezing/heating tests (Fig. 8b and Fig. 8c). The maximum strain decreased from 0.40–0.45 mm/m to 0.30–0.35 mm/m in both tests. On the other, the minimum strains (at –15 °C) obtained in the cyclical-freezing test and in the cyclical-freezing/heating tests, Fig. 8a and Fig. 8c, also decreased over the cycles (from 0.25–0.32 mm/m to 0.30–0.40 mm/m). Finally, the original dimension (at 20 °C) remained constant in the cyclical-heating test (Fig. 8b), but this value slightly decreased from 0 to around –0.04 mm/m in the cyclical-freezing test (Fig. 8a). Overall, slight and almost generalized shrinking was observed. Furthermore, the incorporation of additional C-S-H gel when adding RCA to the mixtures (mortar adhering to the coarser RCA particles, and particles of old mortar within the fine fraction) slightly favored this shrinking phenomenon [23]. For example, the decrease of the maximum strain of mixture SCC0/0 in the cyclical-freezing/heating test was 0.11 mm/m, while this decrease was 0.15 mm/m for mixture SCC100/100. Hence,

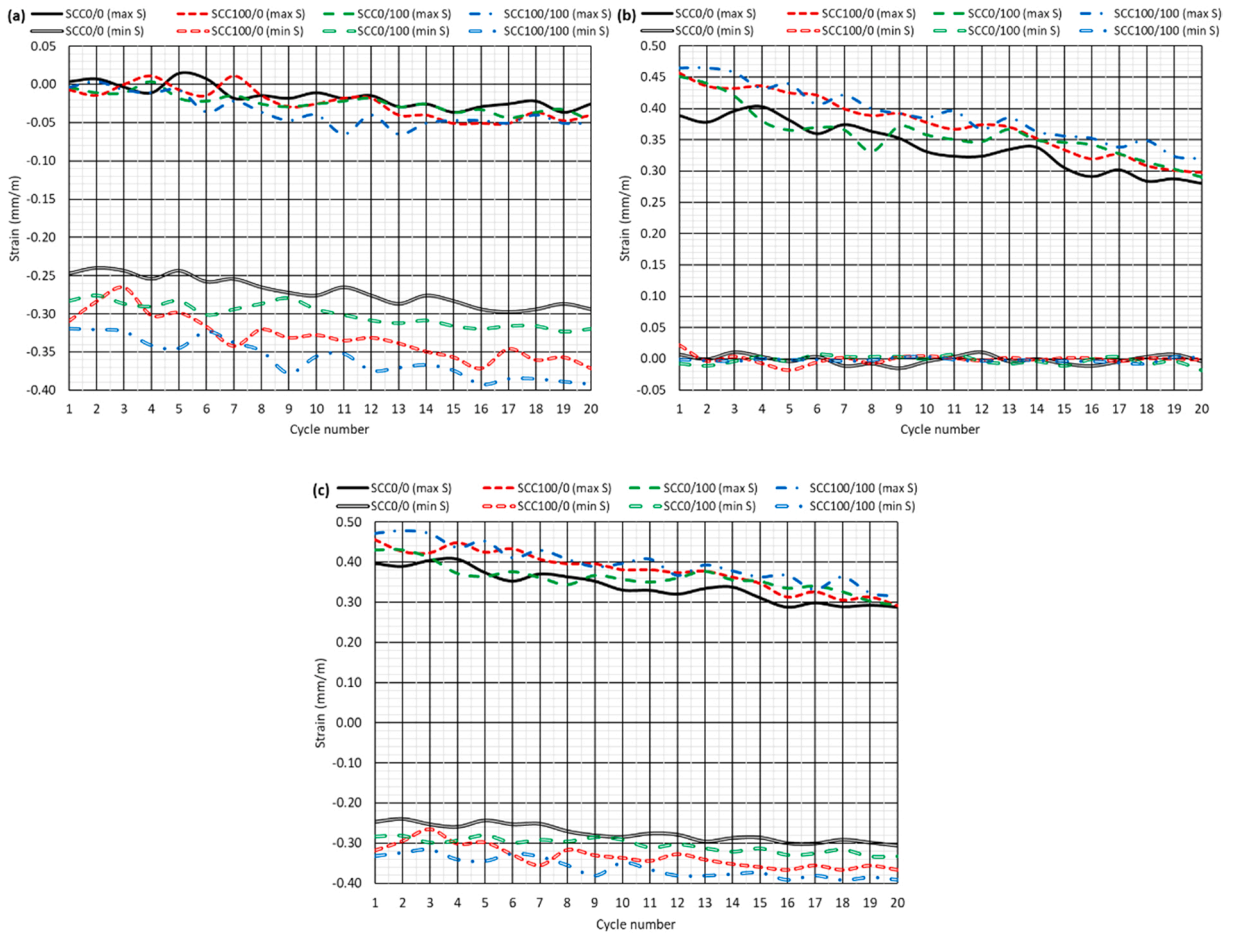


Fig. 8. Maximum (max S) and minimum (min S) strains throughout (a) cyclical-freezing test; (b) cyclical-heating test; (c) cyclical-freezing/heating test.

the justifications have to be mainly centered on physic-chemical reactions within the cementitious matrices.

3.3.2. Linear thermal expansion coefficient

Thermal stress must always be considered in the design of any concrete structure, especially for climates where temperature fluctuations between day and night are high [13]. To estimate this stress, it is necessary to monitor the variation in strain of the concrete within a certain temperature interval. The simplest way to calculate this strain increase is Eq. 1. In this formula, $\Delta\epsilon$ is the increase of strain (m/m), α is the linear thermal expansion coefficient ($^{\circ}\text{C}^{-1}$), and ΔT is the temperature increase ($^{\circ}\text{C}$). Each material has its own linear thermal expansion coefficient [10], the value of which for concrete is between $8 \cdot 10^{-6}$ and $1.2 \cdot 10^{-5} \text{ }^{\circ}\text{C}^{-1}$. Traditionally, $1 \cdot 10^{-5} \text{ }^{\circ}\text{C}^{-1}$ is the linear thermal expansion coefficient used in the design of concrete structures [45]. However, it is advisable to use $1.2 \cdot 10^{-5} \text{ }^{\circ}\text{C}^{-1}$ to achieve greater safety in the calculation of thermal stress in climates with uncertain thermal variations [13].

$$\Delta\epsilon = \alpha \cdot \Delta T \tag{1}$$

Table 4 shows the 95% confidence interval of this coefficient for all mixes, calculated from the results of the constant-temperature tests. As is logical, these values were according to the strain measurements (see Fig. 7). Mixture SCC100/100 had the highest linear thermal expansion coefficient, due to its higher strain in both tests, while mixture SCC0/0 had the lowest one. According to these results, the common value of the linear thermal expansion coefficient, $1 \cdot 10^{-5} \text{ }^{\circ}\text{C}^{-1}$, would be suitable for its use. On the other hand, the

Table 4
95% confidence interval for the linear thermal expansion coefficient obtained in the constant-temperature tests.

	SCC0/0	SCC100/0	SCC0/100	SCC100/100
Freezing test	$7.079 \cdot 10^{-6}$; $7.088 \cdot 10^{-6}$	$8.718 \cdot 10^{-6}$; $8.733 \cdot 10^{-6}$	$8.024 \cdot 10^{-6}$; $8.038 \cdot 10^{-6}$	$9.064 \cdot 10^{-6}$; $9.098 \cdot 10^{-6}$
Heating test	$7.704 \cdot 10^{-6}$; $7.714 \cdot 10^{-6}$	$9.219 \cdot 10^{-6}$; $9.232 \cdot 10^{-6}$	$8.957 \cdot 10^{-6}$; $8.979 \cdot 10^{-6}$	$9.479 \cdot 10^{-6}$; $9.503 \cdot 10^{-6}$

linear thermal expansion coefficient was apparently higher in the heating test in all mixtures with respect to the values registered in the freezing test. However, the expansion of capillary water during the freezing process overlaps the thermal contraction of the concrete. The final result of this overlapping was an apparent linear thermal expansion coefficient that was lower in the frozen region. The chosen value should be therefore the largest of both (heating test).

The linear thermal expansion coefficient obtained cycle-by-cycle from the results of the cyclical-temperature tests (Fig. 9) showed the same effect on each RCA fraction as the coefficient obtained from the results of the constant-temperature tests, as already reported in a previous paper of the authors for the cyclical-freezing and cyclical-heating test [17]. Nevertheless, as expected from the strain values scattering, this coefficient exhibited greater variability in these tests. The coefficient value obtained in the first cycle was very similar to the one obtained in the constant-temperature tests. For subsequent cycles the value of this coefficient showed the same trends as the thermal strain (Fig. 8).

In the cyclical-freezing test, both the minimum and maximum strain decreased over the cycles at a similar rate (Fig. 8a), so the average value of this coefficient remained approximately constant throughout the whole test (Fig. 9a). In Fig. 9b, the trend of the thermal strain in the cyclical heating (Fig. 8b) is also reproduced. Nevertheless, in the cyclical-freezing/heating test, as shown in Fig. 8c, the decrease in minimum strain (at $-15\text{ }^{\circ}\text{C}$) partially compensated the decrease in maximum strain (at $20\text{ }^{\circ}\text{C}$), which reduced any decrease of this coefficient, as depicted in Fig. 9c.

The graphics in Fig. 9, although realistic, are of limited application from an engineering point of view, because their calculation implies that the thermal expansion coefficient is calculated cycle-by-cycle disregarding the concrete strain of previous cycles [17]. However, the effect of this strain is cumulative in a real concrete structure [11], and it is advisable to consider the historic life of the structure when calculating its thermal stress [12]. For this reason, Fig. 10 shows more useful apparent values of the linear thermal expansion coefficient based on the dimensions of the specimen before the test, i.e., at the beginning of the first cycle, taken as the length reference (strain equals to 0 mm/m).

In the cyclical-heating test, Fig. 10b, the linear thermal expansion coefficient followed a decreasing trend similar to that of Fig. 9b, due to an absence of any variations in the minimum strain throughout the test, which was approximately equal to 0 mm/m in all cycles (Fig. 8b). However, this coefficient showed an increasing trend in the cyclical-freezing test, Fig. 10a, due to the decrease in the minimum strain (Fig. 8a). Therefore, the strain variation in the cyclical-freezing test was higher in the last cycles than in the first cycles,

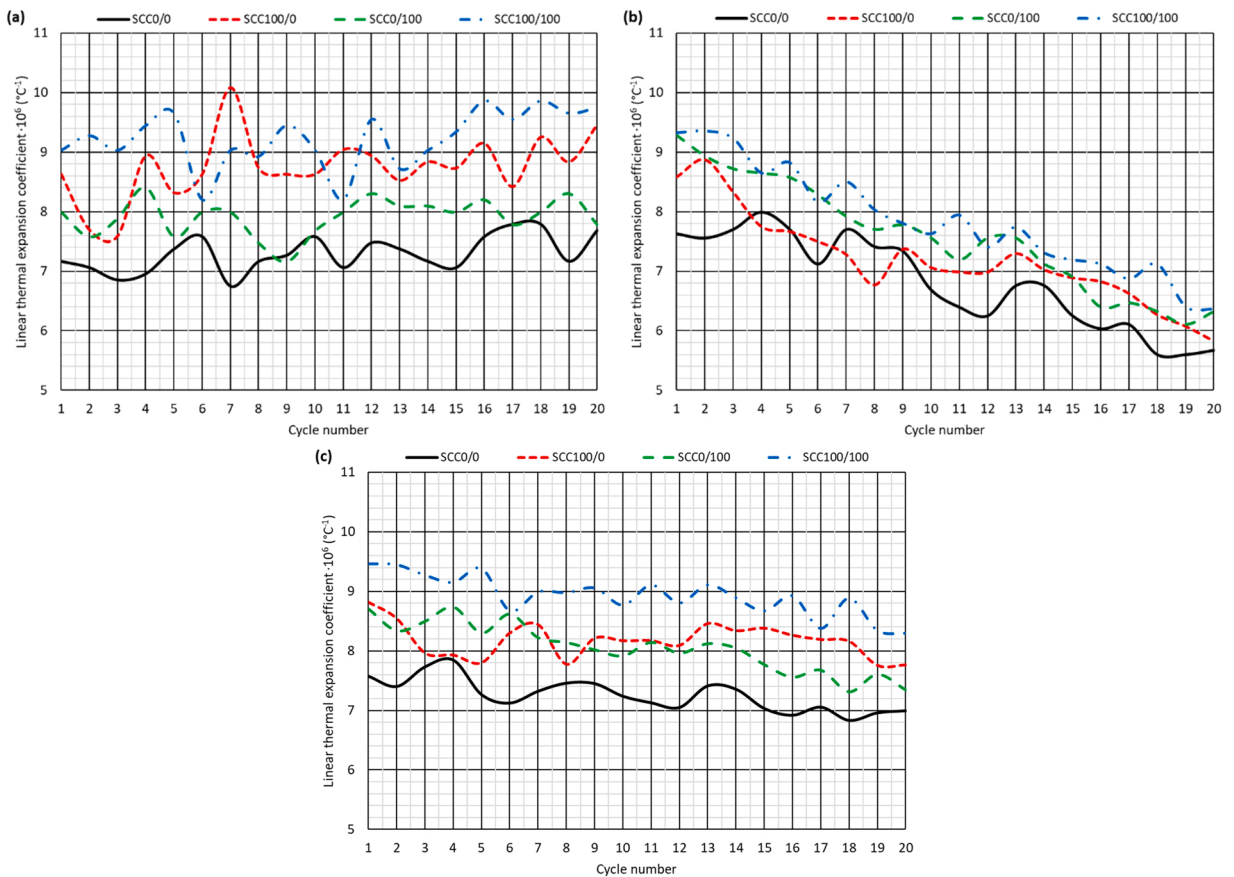


Fig. 9. Thermal expansion coefficient calculated cycle-by-cycle in the (a) cyclical-freezing test; (b) cyclical-heating test; (c) cyclical-freezing/heating test.

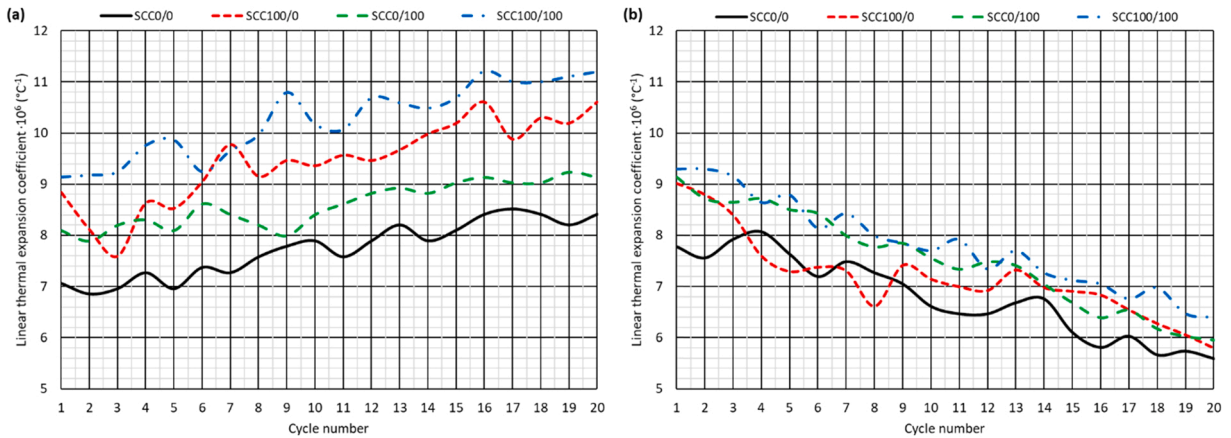


Fig. 10. Linear thermal expansion coefficient obtained through the strain increase in each individual cycle regarding the initial strain (0 mm/m): (a) cyclical-freezing test; (b) cyclical-heating test.

thereby increasing the value of this coefficient.

Despite the complex patterns of the linear thermal expansion coefficient, if a structure manufactured with SCC with RCA is subjected to both constant (positive or negative) and cyclical positive temperature increases (Fig. 7 and Fig. 10b), then the conventional value, $1 \cdot 10^{-5} \text{ } ^\circ\text{C}^{-1}$, could be valid. However, according to the results shown in Fig. 10a, some values of this coefficient during the cyclical-freezing test were slightly higher than $1.1 \cdot 10^{-5} \text{ } ^\circ\text{C}^{-1}$. Therefore, if the structure were located in climates with very low temperatures, even below $0 \text{ } ^\circ\text{C}$, it might be necessary to use the highest value of the interval discussed above, $1.2 \cdot 10^{-5} \text{ } ^\circ\text{C}^{-1}$, as the linear thermal expansion coefficient to ensure the safe calculation of thermal stresses. In line with these results and for the sake of simplicity, a linear thermal expansion coefficient of $1.2 \cdot 10^{-5} \text{ } ^\circ\text{C}^{-1}$ will always be safer to use, regardless of the waste fraction in use and the temperature increase under consideration.

3.4. Internal damage: micro-cracking

Concrete is not a continuous medium, but a composite consisting of cementitious matrix, aggregates, and pores (vacuolar, capillary). Hence, the classical equation for elastic waves (Eq. 2, ν wave velocity, E modulus of elasticity, and ρ density) is illustrative, but not so rigorous. In fact, ultrasonic pulse passing through a concrete mixture is largely conditioned by the continuity of the propagation medium [58], as pores can disrupt this continuity and reduce the UPV signals [59].

$$v = \sqrt{E/\rho} \tag{2}$$

When concrete is subjected to a temperature increase or decrease, each component undergoes a slightly different strain [8]. Furthermore, some of the products formed by the initial binder hydration can be transformed when the temperature rises, usually due to partial loss of water and allotropic changes, which involves volumetric variations at microstructural levels. In the same way, concrete is a porous material with hygroscopic properties, so it absorbs water from the environment that freezes and increases its volume when subjected to temperatures below $0 \text{ } ^\circ\text{C}$ [9].

These above-mentioned phenomena cause internal damage at a microscopic level that consists of variations in the amount and size of the pores, and the appearance of micro-cracks [60]. This micro-cracking has its origin in the ITZs and other weak regions of the concrete microstructure and connect different zones of the cementitious matrix [5]. Based on the mentioned aspects, the cyclical-temperature tests were expected to cause remarkable internal damage to the mixtures.

Determining or quantifying this internal damage in concrete is a complex question, because it cannot be easily evaluated in a direct way, so it is therefore necessary to use indirect measurements most of the time [61]. Modern studies have shown that Ultrasonic Pulse Velocity (UPV), initially related to material stiffness as shown by Eq. 2, can be used to estimate the internal damage of concrete [59]. Although any damage cannot be exactly evaluated, damage to concrete at different time points can be compared [58]. Consequently, in all the cyclical-temperature tests of this research work, the UPV of all the specimens was measured before the start of the test and after each cycle, in order to analyze the evolution of their internal damage. The UPV measurement was performed by the direct method [47] in the longitudinal direction of $75 \times 75 \times 275$ -mm prismatic specimens.

The initial UPV of each mixture is listed in Table 5. The measured values were fairly consistent with the initial mechanical

Table 5
Initial UPV of the SCC mixtures.

	SCC0/0	SCC100/0	SCC0/100	SCC100/100
UPV (km/s)	4.04	3.69	3.41	2.76

properties in Section 3.2, as shown in Fig. 11. Highly accurate linear relationships were obtained.

This test was not applied to analyze the constant-temperature tests, due to the low significance of the results. UPV evolution throughout each cyclical-temperature test is shown in Fig. 12, highlighting the differences between each test and each mixture:

- The decrease in UPV was four times greater in the tests in which temperatures below 0 °C were reached: 15–20% compared to 4–5% in the cyclical-heating tests after the 20th cycle. The internal damage after heating (incipient decomposition of hydration products) was notably smaller than that obtained after the freezing cycles (mechanical breakage by capillary water expansion after freezing). In contrast, the decrease in UPV was more progressive in the cyclical-heating test, although it was less pronounced before the 7th cycle and more marked from the 7th to the 20th cycle.
- In both cyclical-freezing and cyclical-freezing/heating tests, the UPV during the first 14 cycles remained practically constant, only undergoing small fluctuations, due to the intrinsic variability of the UPV measurements [25]. In subsequent cycles, the decrease of the UPV was very noticeable, as the concrete specimens suffered severe micro-cracking from the 13th cycle.
- The internal damage experienced by the mixtures was greater when coarse RCA was added. Less damage within mixtures SCC0/0 and SCC0/100 than within mixtures SCC100/0 and SCC100/100 is therefore an intuitive observation. It is likely that the weak ITZs generated by the RCA coarse fraction favored the appearance of micro-cracks [14].

Finally, it is important to note that the damage suffered by specimens in these tests was greater than it might otherwise be in a real structure, and, therefore, the increased resistance to UPV of the specimens in these tests was greater than it might be in a real structure [61]. This difference was due to the fact that the real structures were not subjected to such large temperature increases [52]. In addition, the inside of the structure reached much lower temperatures than the outside, due to its large dimensions [60]. Nevertheless, the results obtained offer an overview of the effect of RCA on the thermal micro-cracking of SCC.

3.5. Loss of compressive strength

All the observations discussed in the previous sections, especially micro-cracking, can reduce the strength of concrete [20]. Each original 75×75×275-mm prismatic specimen was cut after removing the strain gauges, to evaluate the variation of compressive strength after each thermal test, thereby obtaining two 75×75×75-mm cubic specimens, as shown in Fig. 13. In addition, the load was applied on the cut-off faces (in red in Fig. 13) during the compressive-strength test, to reproduce the skin effect on lateral faces of these cubic specimens that occurs when testing standardized specimens [13]. For this reason, the cut faces were polished (faced) to ensure that they were completely flat, without any irregularity. Thus, the compressive strength after each thermal test was measured on four 75-mm cubic specimens (as indicated in Section 2.3.1, each thermal test was performed on two 75×75×275-mm prismatic specimens). Furthermore, the undamaged 75×75×275-mm prismatic specimen was cut and polished to obtain two 75×75×75-mm cubic specimens, in order to obtain the compressive strength of concrete not subjected to the thermal tests on the same type of specimen. Thus, all the values of compressive strength were perfectly comparable to each other.

Fig. 14 shows the compressive strength of each mixture after each thermal test, while Table 6 shows the percentage loss of strength. The values obtained were in line with the cause-and-effect analysis of the internal damage described in the previous section:

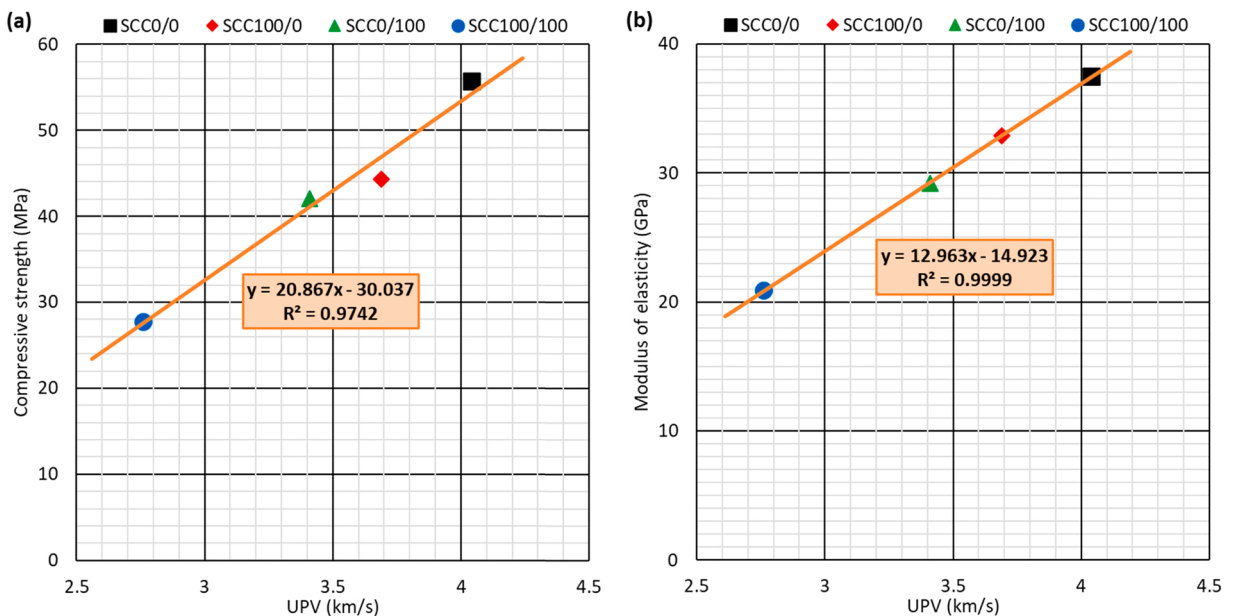


Fig. 11. Relationship between the UPV and (a) compressive strength; (b) modulus of elasticity.

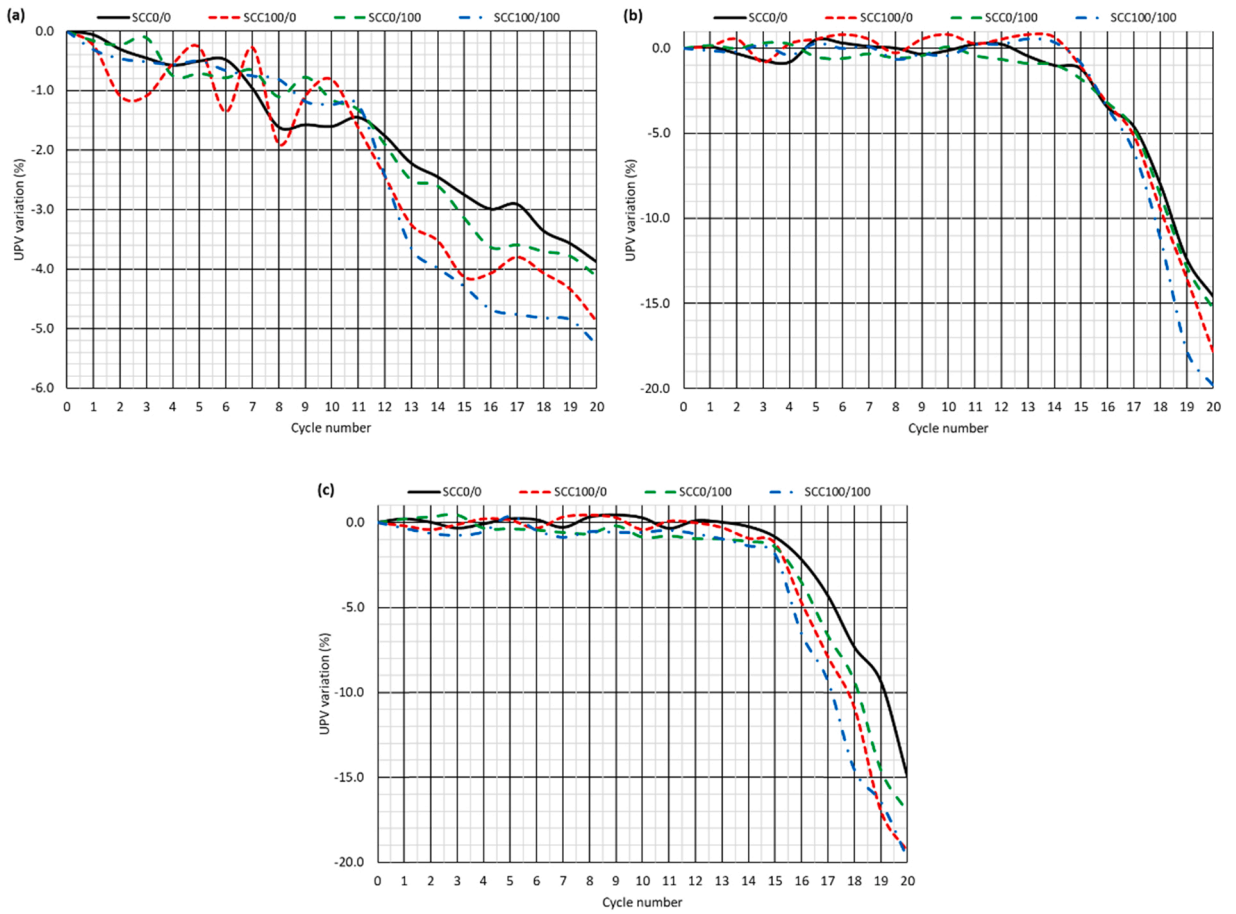


Fig. 12. UPV evolution throughout (a) cyclical-heating test; (b) cyclical-freezing test; (c) cyclical freezing/heating test.

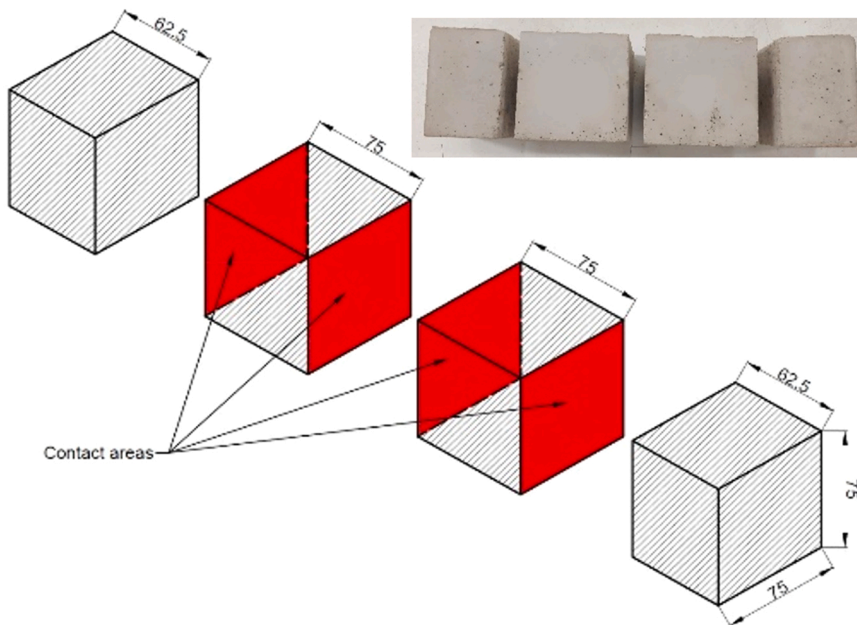


Fig. 13. Original specimens cut to obtain the cubic specimens for the compressive-strength test. Dimensions in mm.

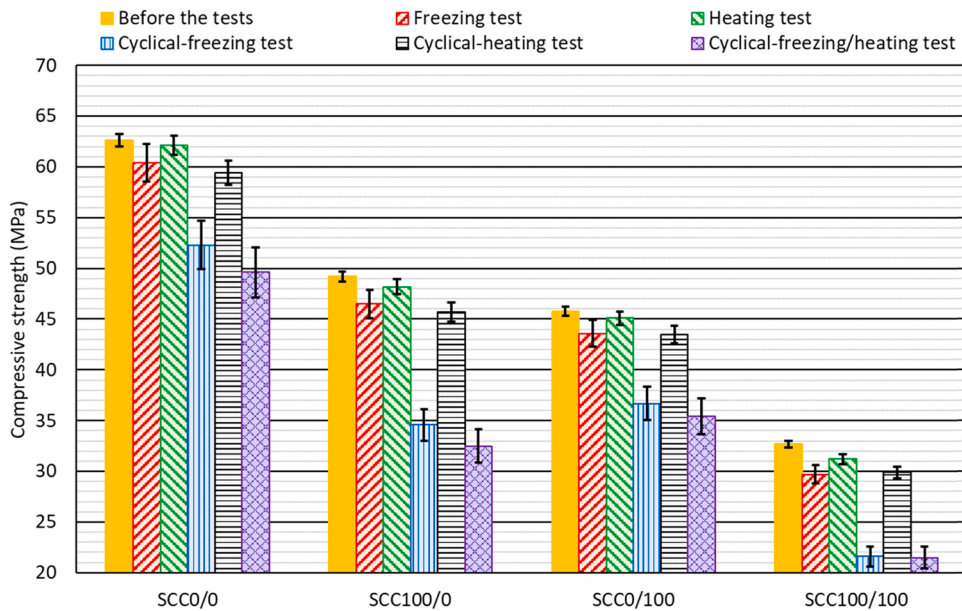


Fig. 14. Compressive strength of each mixture after each test. Cubic specimens.

Table 6

Loss of compressive strength (%) of each mixture after each test.

	SCC0/0	SCC100/0	SCC0/100	SCC100/100
Freezing test	3.5	5.5	4.8	9.2
Heating test	0.8	2.0	1.5	4.6
Cyclical-freezing test	16.5	29.7	19.9	33.9
Cyclical-heating test	5.1	7.1	5.0	8.6
Cyclical-freezing/heating test	20.8	33.9	22.7	34.3

- On the one hand, the decrease in compressive strength caused by both constant-temperature tests was appreciable in all mixes, although it was more considerable in the freezing test (losses from 3.5% to 9.2%) than in heating test (losses from 0.8% to 4.6%). Micro-cracking due to freezing was more severe than the heating damage in the experimental conditions of these tests.
- The negative effect of the cyclical-temperature tests was greater in all mixes (including the reference mixture), than in constant-temperature tests, especially in those tests in which temperatures below 0 °C were reached. As the internal damage during the cyclical-heating test was lower, the loss of compressive strength it produced was less notable (from 5.1% to 8.6%). The decrease of the strength values was higher in both the cyclical-freezing and cyclical-freezing/heating tests (from 16.5% to 34.3%). Furthermore, the higher dispersion of the experimental measures of both tests reflected a less reliable behavior of the mixtures.
- Regarding the mixtures, the higher the content of RCA, the higher the decrease of specimen compressive strength. Mixture SCC100/100 therefore showed the highest strength loss, reaching 8.6% in the cyclical-heating test and 33.9% and 34.3% in the cyclical-freezing test and cyclical-freezing/heating test, respectively. Furthermore, if the results for mixtures SCC100/0 and SCC0/100 are compared, it can be concluded that the addition of coarse RCA was more harmful than the use of fine RCA. The internal damage of SCC100/0 was more notable in all cases.

3.6. Hygroscopicity

Hygroscopicity is the capability of a material to adsorb/absorb atmospheric moisture, *i.e.*, water vapor [62]. In hydraulic mixtures, this property fundamentally depends on the surface porosity of the material, as well as the continuity of its pore network [63]. The weight variation of concrete, although very small because of the low porosity of its skin [62], is the main control measure of hygroscopicity. It is even lower in SCC, because its high flowability leaves a more continuous skin [30]. However, this property can produce harmful effects on concrete. On the one hand, if concrete is subjected to temperatures below 0 °C, the water vapor that has been absorbed freezes and increases in volume, which favors progressive micro-cracking [64]. On the other hand, the equilibrium vapor/micro-drops of water can carry harmful compounds such as chlorides or sulfates, especially in marine environments, which can affect the concrete durability [65]. This issue is also aesthetically important, especially in fiber-reinforced concrete, as the corrosion of metallic fibers causes the darkening of the concrete surface, and even the appearance of flaking [66].

The specimens were weighed at the end of each phase of the cyclical-temperature tests, in order to measure this property, *i.e.*, at the

entrance and exit of the freezer or oven. In this way, the weight variation of the specimens after each cycle could be calculated. The results obtained are shown in Fig. 15.

The weight variation was approximately double in the cyclical-heating test than in both the cyclical-freezing and the cyclical-freezing/heating tests, due to the fact that the water vapor absorption was higher when the concrete was cooled from 70 °C to ambient temperature [66]. In the cyclical-freezing test, rather than cooling them, the specimens were heated during the ambient-temperature phase, and, therefore, a liquid film of water condensation coated the surface and reduced their vapor absorption capacity [66]. In the cyclical-freezing/heating test, the cooling of the specimen after the heating oven phase took place in a freezer, at - 15 °C, and water vapor was absorbed by the concrete to a lesser extent [67]. The increase in hygroscopicity over the cycles was clear in all cases, due to the surface damage to the concrete during these tests: the new cracks and pores that surfaced over the cycles favored the entry of water vapor [68].

Mixture SCC100/100 (higher w/b ratio, hence greater porosity) demonstrated the highest weight variations, followed by the mixture SCC0/100 (100% fine RCA). As shown in the former section, the micro-cracking of mixture SCC100/0 was higher than in mixture SCC0/100 when temperatures below 0 °C were reached. This led to higher weight variations in mixture SCC100/0 than in mixture SCC0/100 in the last cycles of the cyclical-freezing and cyclical-freezing/heating tests (Fig. 15b and Fig. 15c).

4. Conclusions

Throughout this article, the fresh and hardened behavior of Self-Compacting Concrete (SCC) made with 100% coarse and/or fine Recycled Concrete Aggregate (RCA) has been evaluated. On the one hand, if the amount of the finest particles of the aggregates and the effective water-to-binder ratio are adjusted, a fast-mixing process has been proven to obtain a high-flowability SCC (slump-flow class SF3) with high amounts of coarse and fine RCA. On the other hand, it has been demonstrated that an accurate linear relationship between compressive strength, modulus of elasticity, and UPV in these sorts of RCA mixes can be established. All these properties were worsened when adding coarse or fine RCA, although the joint incorporation of both fractions was the most negative situation. However, the great novelty of this research work is linked to the thermal tests, in which the mixtures were subjected to both positive and negative and both constant and cyclical temperature increases. The following conclusions can be drawn from these thermal tests:

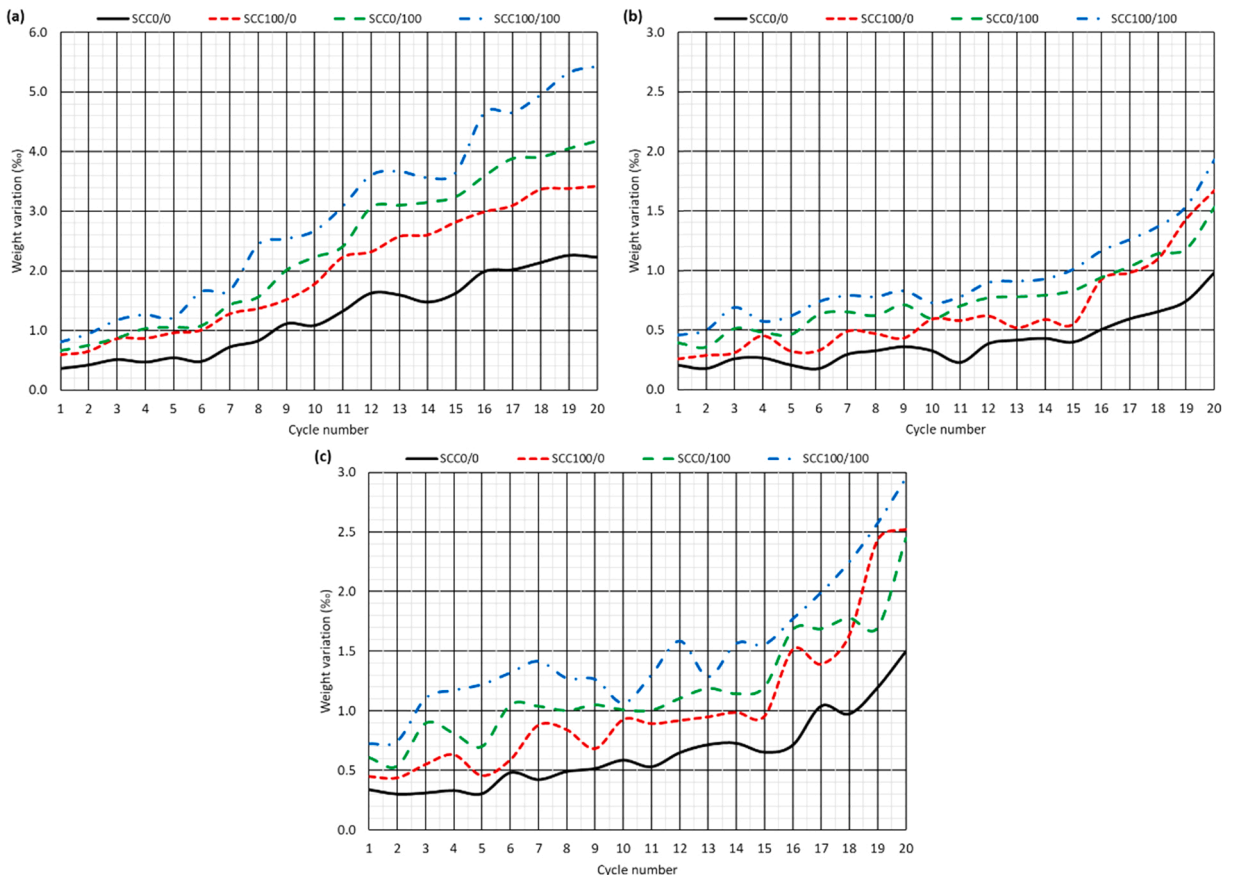


Fig. 15. Weight variation (%) of the specimens in each cycle of (a) cyclical-heating test; (b) cyclical-freezing test; (c) cyclical-freezing/heating test.

- The thermal deformability of SCC under a constant temperature was increased by the addition of RCA, the coarse fraction of which had a greater effect. The deformability of all mixtures was higher under a positive temperature variation (higher than 0 °C), regardless of the RCA fraction used.
- Both coarse and fine RCA had the same effect on the thermal deformability of SCC under cyclical temperature variations, regardless of its (positive or negative) sign. On the one hand, the maximum strain experienced by the concrete under positive (higher than 0 °C) temperature variations decreased over the cycles. On the other hand, a negative remaining strain appeared under negative temperature variations (below 0 °C). Coarse RCA had a more notable effect, probably due to the increase of old mortar in the SCC following its addition.
- It is safer to use $1.2 \cdot 10^{-5} \text{ } ^\circ\text{C}^{-1}$ as the linear thermal expansion coefficient instead of $1 \cdot 10^{-5} \text{ } ^\circ\text{C}^{-1}$ when estimating the thermal stress of a structure manufactured with SCC that incorporates RCA. In this way, the effects caused by the addition of this by-product, such as the increase of both the thermal deformability and the shortening of concrete under cyclical temperature variations, may be safely estimated.
- The application of cyclical temperature variations, especially when temperatures below 0 °C were reached, resulted in generalized micro-cracking of the specimens and led to a notable decrease in the UPV and the compressive strength. The increase of porosity caused by the addition of RCA increased this damage, although the poor-quality interfacial transition zones of coarse RCA had a more detrimental effect on its evolution.
- Although the evolution of the hygroscopicity of SCC over the cycles was low, it was increased when adding RCA, due to the increased porosity of the SCC following the addition of this alternative aggregate. Micro-cracking caused by cyclical temperature variations quadrupled the water vapor absorption of the SCC manufactured with RCA at the end of the tests in comparison with the initial values.

Declaration of Competing Interest

The authors declare that they have no known competing financial interests or personal relationships that could have appeared to influence the work reported in this paper.

Acknowledgments

The authors wish to express their gratitude for funding this research work to: the Spanish Ministry of Universities, MICINN, AEI, EU and ERDF [PID2020-113837RB-I00; PID2021-124203OB-I00; RTI2018-097079-B-C31; 10.13039/501100011033; FPU17/03374]; the Junta de Castilla y León (Regional Government) and ERDF [UIC-231, BU119P17]; the Basque Regional Government through the consolidated research group SAREN [IT1619-22]; Youth Employment Initiative (JCyL) and ESF [UBU05B_1274]; and the University of Burgos [Y135. GI].

Conflict of interest

The authors declare that there is no conflict of interest.

References

- [1] J.T. San-José, J.M. Manso, Fiber-reinforced polymer bars embedded in a resin concrete: Study of both materials and their bond behavior, *Polym. Compos.* 27 (3) (2006) 315–322, <https://doi.org/10.1002/pc.20188>.
- [2] S. Cabrera, A. González, R. Rotondaro, Compressive strength in compressed earth blocks. Comparison between different test methods, *Inf. Constr.* 72 (560) (2020) 1–12, <https://doi.org/10.3989/ic.70462>.
- [3] A. Santamaría, J.J. González, M.M. Losáñez, M. Skaf, V. Ortega-López, The design of self-compacting structural mortar containing steelmaking slags as aggregate, *Cem. Concr. Compos.* 111 (2020), 103627, <https://doi.org/10.1016/j.cemconcomp.2020.103627>.
- [4] R. Lanti, M. Martínez, Biaxial bending and axial load in reinforced concrete sections. Numerical approach, *Inf. Constr.* 72 (558) (2020) 1–9, <https://doi.org/10.3989/ic.69148>.
- [5] H. Sogbossi, J. Verdier, S. Multon, Permeability and damage of partially saturated concrete exposed to elevated temperature, *Cem. Concr. Compos.* 109 (2020), 103563, <https://doi.org/10.1016/j.cemconcomp.2020.103563>.
- [6] C. Wang, M. Zhang, Q. Wang, R. Zhang, W. Pei, Y. Zhou, Influence of nano-silica on the performances of concrete under the negative-temperature curing condition, *Cold Reg. Sci. Technol.* 191 (2021), 103357, <https://doi.org/10.1016/j.coldregions.2021.103357>.
- [7] H.Y. Aruntaş, S. Cemalgil, O. Şimşek, G. Durmuş, M. Erdal, Effects of super plasticizer and curing conditions on properties of concrete with and without fiber, *Mater. Lett.* 62 (19) (2008) 3441–3443, <https://doi.org/10.1016/j.matlet.2008.02.064>.
- [8] N. Belayachi, C. Mallet, M. El Marzak, Thermally-induced cracks and their effects on natural and industrial geomaterials, *J. Build. Eng.* 25 (2019), 100806, <https://doi.org/10.1016/j.jobe.2019.100806>.
- [9] V. Ortega-López, J.A. Fuente-Alonso, A. Santamaría, J.T. San-José, Á. Aragón, Durability studies on fiber-reinforced EAF slag concrete for pavements, *Constr. Build. Mater.* 163 (2018) 471–481, <https://doi.org/10.1016/j.conbuildmat.2017.12.121>.
- [10] J.T. Smith, S.L. Tighe, Recycled concrete aggregate coefficient of thermal expansion: Characterization, variability, and impacts on pavement performance, *Transp. Res. Rec.* 2113 (1) (2009) 53–61, <https://doi.org/10.3141/2113-07>.
- [11] S. Fan, Y. Zhang, K.H. Tan, Experimental and analytical studies of reinforced concrete short beams at elevated temperatures, *Eng. Struct.* 212 (2020), 110445, <https://doi.org/10.1016/j.engstruct.2020.110445>.
- [12] M. Li, W. Si, S. Du, M. Zhang, Q. Ren, Y. Shen, Thermal deformation coordination analysis of CC-RCC combined dam structure during construction and operation periods, *Eng. Struct.* 213 (2020), 110587, <https://doi.org/10.1016/j.engstruct.2020.110587>.
- [13] EC-2, Eurocode 2: Design of concrete structures. Part 1-1: General rules and rules for buildings, CEN (European Committee for Standardization), 2010.
- [14] M. Abed, R. Nemes, E. Lublój, Performance of self-compacting high-performance concrete produced with waste materials after exposure to elevated temperature, *J. Mater. Civ. Eng.* 32 (1) (2020), 05019004, [https://doi.org/10.1061/\(ASCE\)MT.1943-5533.0002989](https://doi.org/10.1061/(ASCE)MT.1943-5533.0002989).

- [15] A. Santamaría, A. Orbe, M.M. Losañez, M. Skaf, V. Ortega-Lopez, J.J. González, Self-compacting concrete incorporating electric arc-furnace steelmaking slag as aggregate, *Mater. Des.* 115 (2017) 179–193, <https://doi.org/10.1016/j.matdes.2016.11.048>.
- [16] S. Santos, P.R. da Silva, J. de Brito, Self-compacting concrete with recycled aggregates – A literature review, *J. Build. Eng.* 22 (2019) 349–371, <https://doi.org/10.1016/j.jobte.2019.01.001>.
- [17] V. Revilla-Cuesta, M. Skaf, J.A. Chica, J.A. Fuente-Alonso, V. Ortega-López, Thermal deformability of recycled self-compacting concrete under cyclical temperature variations, *Mater. Lett.* 278 (2020), 128417, <https://doi.org/10.1016/j.matlet.2020.128417>.
- [18] P. Uthachotirat, P. Sukontasukkul, P. Jitsangiam, C. Suksiripattananong, V. Sata, P. Chindaprasit, Thermal and sound properties of concrete mixed with high porous aggregates from manufacturing waste impregnated with phase change material, *J. Build. Eng.* 29 (2020), 101111, <https://doi.org/10.1016/j.jobte.2019.101111>.
- [19] V. Lesovik, V. Voronov, E. Glagolev, R. Fediuk, A. Alashkanov, Y.H.M. Amran, G. Murali, A. Baranov, Improving the behaviors of foam concrete through the use of composite binder, *J. Build. Eng.* 31 (2020), 101414, <https://doi.org/10.1016/j.jobte.2020.101414>.
- [20] Y. Zhang, J.W. Ju, Q. Chen, Z. Yan, H. Zhu, Z. Jiang, Characterizing and analyzing the residual interfacial behavior of steel fibers embedded into cement-based matrices after exposure to high temperatures, *Compos. Part B: Eng.* 191 (2020), 107933, <https://doi.org/10.1016/j.compositesb.2020.107933>.
- [21] C. Laneyrie, A.L. Beaucour, M.F. Green, R.L. Hebert, B. Ledesert, A. Noumowe, Influence of recycled coarse aggregates on normal and high performance concrete subjected to elevated temperatures, *Constr. Build. Mater.* 111 (2016) 368–378, <https://doi.org/10.1016/j.conbuildmat.2016.02.056>.
- [22] B. Cantero, M. Bravo, J. de Brito, I.F.S. del Bosque, C. Medina, Thermal performance of concrete with recycled concrete powder as partial cement replacement and recycled CDW aggregate, *Appl. Sci.* 10 (13) (2020) 4540, <https://doi.org/10.3390/app10134540>.
- [23] A.R. Khan, S. Fareed, M.S. Khan, Use of recycled concrete aggregates in structural concrete, *Sustain. Constr. Mater. Technol.* 2 (2019).
- [24] E.A. Ohemeng, S.O. Ekololu, Comparative analysis on costs and benefits of producing natural and recycled concrete aggregates: A South African case study, *Case Stud. Constr. Mater.* 13 (2020), e00450, <https://doi.org/10.1016/j.cscm.2020.e00450>.
- [25] F. Fiol, C. Thomas, C. Muñoz, V. Ortega-López, J.M. Manso, The influence of recycled aggregates from precast elements on the mechanical properties of structural self-compacting concrete, *Constr. Build. Mater.* 182 (2018) 309–323, <https://doi.org/10.1016/j.conbuildmat.2018.06.132>.
- [26] A. Gonzalez-Corominas, M. Itxerria, Effects of using recycled concrete aggregates on the shrinkage of high performance concrete, *Constr. Build. Mater.* 115 (2016) 32–41, <https://doi.org/10.1016/j.conbuildmat.2016.04.031>.
- [27] T. Gonçalves, R.V. Silva, J. de Brito, J.M. Fernández, A.R. Esquinas, Mechanical and durability performance of mortars with fine recycled concrete aggregates and reactive magnesium oxide as partial cement replacement, *Cem. Concr. Compos.* 105 (2020), 103420, <https://doi.org/10.1016/j.cemconcomp.2019.103420>.
- [28] M. Bravo, J. de Brito, L. Evangelista, J. Pacheco, Durability and shrinkage of concrete with CDW as recycled aggregates: Benefits from superplasticizer's incorporation and influence of CDW composition, *Constr. Build. Mater.* 168 (2018) 818–830, <https://doi.org/10.1016/j.conbuildmat.2018.02.176>.
- [29] R.V. Silva, J. de Brito, R.K. Dhir, Fresh-state performance of recycled aggregate concrete: A review, *Constr. Build. Mater.* 178 (2018) 19–31, <https://doi.org/10.1016/j.conbuildmat.2018.05.149>.
- [30] V. Revilla-Cuesta, M. Skaf, F. Faleschini, J.M. Manso, V. Ortega-López, Self-compacting concrete manufactured with recycled concrete aggregate: An overview, *J. Clean. Prod.* 262 (2020), 121362, <https://doi.org/10.1016/j.jclepro.2020.121362>.
- [31] J. Nobre, M. Bravo, J. de Brito, G. Duarte, Durability performance of dry-mix shotcrete produced with coarse recycled concrete aggregates, *J. Build. Eng.* 29 (2020), 101135, <https://doi.org/10.1016/j.jobte.2019.101135>.
- [32] R.V. Silva, J. De Brito, R.K. Dhir, The influence of the use of recycled aggregates on the compressive strength of concrete: A review, *Eur. J. Environ. Civ. Eng.* 19 (7) (2015) 825–849, <https://doi.org/10.1080/19648189.2014.974831>.
- [33] V. Revilla-Cuesta, V. Ortega-López, M. Skaf, J.M. Manso, Effect of fine recycled concrete aggregate on the mechanical behavior of self-compacting concrete, *Constr. Build. Mater.* 263 (2020), 120671, <https://doi.org/10.1016/j.conbuildmat.2020.120671>.
- [34] L. Evangelista, J. De Brito, Concrete with fine recycled aggregates: A review, *Eur. J. Environ. Civ. Eng.* 18 (2) (2014) 129–172, <https://doi.org/10.1080/19648189.2013.851038>.
- [35] B. Xiong, C. Demartino, J. Xu, A. Simi, G.C. Marano, Y. Xiao, High-strain rate compressive behavior of concrete made with substituted coarse aggregates: Recycled crushed concrete and clay bricks, *Constr. Build. Mater.* 301 (2021), 123875, <https://doi.org/10.1016/j.conbuildmat.2021.123875>.
- [36] J.A. Larbi, W.M.M. Heijnen, J.P. Brouwer, E. Mulder, Preliminary laboratory investigation of thermally treated recycled concrete aggregate for general use in concrete, *Waste Manag. Ser.* 1 (2000) 129–139, [https://doi.org/10.1016/S0713-2743\(00\)80025-2](https://doi.org/10.1016/S0713-2743(00)80025-2).
- [37] J. Xu, X. Zhao, Y. Yu, T. Xie, G. Yang, J. Xue, Parametric sensitivity analysis and modelling of mechanical properties of normal- and high-strength recycled aggregate concrete using grey theory, multiple nonlinear regression and artificial neural networks, *Constr. Build. Mater.* 211 (2019) 479–491, <https://doi.org/10.1016/j.conbuildmat.2019.03.234>.
- [38] S.M.S. Kazmi, M.J. Munir, Y.F. Wu, I. Patnaikuni, Y. Zhou, F. Xing, Effect of different aggregate treatment techniques on the freeze-thaw and sulfate resistance of recycled aggregate concrete, *Cold Reg. Sci. Technol.* 178 (2020), 103126, <https://doi.org/10.1016/j.coldregions.2020.103126>.
- [39] M. Šefflová, M. Volf, T. Pavlí, Thermal properties of concrete with recycled aggregate, *Adv. Mater. Res* 1054 (2014) 227–233, <https://doi.org/10.4028/www.scientific.net/AMR.1054.227>.
- [40] H. Zhao, F. Liu, H. Yang, Residual compressive response of concrete produced with both coarse and fine recycled concrete aggregates after thermal exposure, *Constr. Build. Mater.* 244 (2020), 118397, <https://doi.org/10.1016/j.conbuildmat.2020.118397>.
- [41] N. Garcia-Troncoso, L. Li, Q. Cheng, K.H. Mo, T.C. Ling, Comparative study on the properties and high temperature resistance of self-compacting concrete with various types of recycled aggregates, *Case Stud. Constr. Mater.* 15 (2021), e00678, <https://doi.org/10.1016/j.cscm.2021.e00678>.
- [42] H. Zhao, Y. Wang, F. Liu, Stress-strain relationship of coarse RCA concrete exposed to elevated temperatures, *Mag. Concr. Res.* 69 (13) (2017) 649–664, <https://doi.org/10.1680/jmacr.16.00333>.
- [43] X. Hu, Q. Lu, Z. Xu, W. Zhang, S. Cheng, Compressive stress-strain relation of recycled aggregate concrete under cyclic loading, *Constr. Build. Mater.* 193 (2018) 72–83, <https://doi.org/10.1016/j.conbuildmat.2018.10.137>.
- [44] B. Li, S. Dai, Y. Zhan, J. Xu, X. Guo, Y. Yang, Y. Chen, Strength criterion of recycled aggregate concrete under triaxial compression: Model calibration, *Constr. Build. Mater.* 320 (2022), 126201, <https://doi.org/10.1016/j.conbuildmat.2021.126201>.
- [45] H. Zhao, F. Liu, H. Yang, Thermal properties of coarse RCA concrete at elevated temperatures, *Appl. Therm. Eng.* 140 (2018) 180–189, <https://doi.org/10.1016/j.applthermaeng.2018.05.032>.
- [46] M. Bravo, J. de Brito, L. Evangelista, Thermal performance of concrete with recycled aggregates from CDW plants, *Appl. Sci.* 7 (7) (2017) 740, <https://doi.org/10.3390/app7070740>.
- [47] M. Omrane, M. Rabehi, Effect of natural pozzolan and recycled concrete aggregates on thermal and physico-mechanical characteristics of self-compacting concrete, *Constr. Build. Mater.* 247 (2020), 118576, <https://doi.org/10.1016/j.conbuildmat.2020.118576>.
- [48] EFNARC, Specification Guidelines for Self-compacting Concrete, European Federation of National Associations Representing producers and applicators of specialist building products for Concrete, 2002.
- [49] EN-Euronorm, Rue de stassart, 36. Belgium-1050 Brussels, European Committee for Standardization.
- [50] I. González-Taboada, B. González-Fontebao, J. Eiras-López, G. Rojo-López, Tools for the study of self-compacting recycled concrete fresh behaviour: Workability and rheology, *J. Clean. Prod.* 156 (2017) 1–18, <https://doi.org/10.1016/j.jclepro.2017.04.045>.
- [51] M.I. Dieste-Velasco, M. Díez-Mediavilla, D. Granados-López, D. González-Peña, C. Alonso-Tristán, Performance of global luminous efficacy models and proposal of a new model for daylighting in Burgos, Spain, *Renew. Energy* 133 (2019) 1000–1010, <https://doi.org/10.1016/j.renene.2018.10.085>.
- [52] C. Viceto, S.C. Pereira, A. Rocha, Climate change projections of extreme temperatures for the Iberian Peninsula, *Atmosphere* 10 (5) (2019) 229, <https://doi.org/10.3390/atmos10050229>.
- [53] T. Yao, X. Zhang, H. Guan, H. Zhou, M. Hua, X. Wang, Climatic and environmental controls on stable isotopes in atmospheric water vapor near the surface observed in Changsha, China, *Atmos. Environ.* 189 (2018) 252–263, <https://doi.org/10.1016/j.atmosenv.2018.07.008>.

- [54] A.L. Beaucour, P. Pliya, F. Faleschini, R. Njinwoua, C. Pellegrino, A. Noumowé, Influence of elevated temperature on properties of radiation shielding concrete with electric arc furnace slag as coarse aggregate, *Constr. Build. Mater.* 256 (2020), 119385, <https://doi.org/10.1016/j.conbuildmat.2020.119385>.
- [55] E. Güneysi, M. Gesoğlu, Z. Algin, H. Yazici, Effect of surface treatment methods on the properties of self-compacting concrete with recycled aggregates, *Constr. Build. Mater.* 64 (2014) 172–183, <https://doi.org/10.1016/j.conbuildmat.2014.04.090>.
- [56] O. Kebaili, M. Mouret, N. Arabia, F. Cassagnabere, Adverse effect of the mass substitution of natural aggregates by air-dried recycled concrete aggregates on the self-compacting ability of concrete: Evidence and analysis through an example, *J. Clean. Prod.* 87 (1) (2015) 752–761, <https://doi.org/10.1016/j.jclepro.2014.10.077>.
- [57] S.C. Kou, C.S. Poon, Properties of self-compacting concrete prepared with coarse and fine recycled concrete aggregates, *Cem. Concr. Compos.* 31 (9) (2009) 622–627, <https://doi.org/10.1016/j.cemconcomp.2009.06.005>.
- [58] Y. Boukari, D. Bulteel, P. Rivard, N.E. Abriak, Combining nonlinear acoustics and physico-chemical analysis of aggregates to improve alkali-silica reaction monitoring, *Cem. Concr. Res.* 67 (2015) 44–51, <https://doi.org/10.1016/j.cemconres.2014.08.005>.
- [59] A. Aseem, W. Latif Baloch, R.A. Khushnood, A. Mushtaq, Structural health assessment of fire damaged building using non-destructive testing and micro-graphical forensic analysis: A case study, *Case Stud. Constr. Mater.* 11 (2019), e00258, <https://doi.org/10.1016/j.cscm.2019.e00258>.
- [60] L. Shen, Q. Ren, G. Cusatis, M. Cao, L. Xu, Y. Yang, Numerical study on crack thermal resistance effect on thermo-mechanical coupled behavior of concrete structure at room temperature, *Int. J. Solids Struct.* 182–183 (2020) 141–155, <https://doi.org/10.1016/j.ijsolstr.2019.07.031>.
- [61] R. Al-Rousan, Behavior of strengthened concrete beams damaged by thermal shock, *Mag. Civ. Eng.* 94 (2) (2020) 93–107, <https://doi.org/10.18720/MCE.94.8>.
- [62] A. Al-Mohamadawi, K. Benhabib, R.M. Dheilily, A. Goullieux, Hygric behavior of cement composites elaborated with flax shives, a byproduct of the ainen industry, *Waste Biomass Valor.* 11 (9) (2020) 5053–5066, <https://doi.org/10.1007/s12649-019-00798-4>.
- [63] A.D. Trindade, G.B.A. Coelho, F.M.A. Henriques, Influence of the climatic conditions on the hygrothermal performance of autoclaved aerated concrete masonry walls, *J. Build. Eng.* 33 (2021), 101578, <https://doi.org/10.1016/j.jobe.2020.101578>.
- [64] Y. Wang, J. Huang, D. Wang, Y. Liu, Z. Zhao, J. Liu, Experimental study on hygrothermal characteristics of coral sand aggregate concrete and aerated concrete under different humidity and temperature conditions, *Constr. Build. Mater.* 230 (2020), 117034, <https://doi.org/10.1016/j.conbuildmat.2019.117034>.
- [65] F.M. Mukhtar, O. Arowojolu, Recent developments in experimental and computational studies of hygrothermal effects on the bond between FRP and concrete, *J. Reinf. Plast. Compos.* 39 (11–12) (2020) 422–442, <https://doi.org/10.1177/0731684420912332>.
- [66] G. Velayutham, C.B. Cheah, The effects of steel fibre on the mechanical strength and durability of steel fibre reinforced high strength concrete (SFRHC) subjected to normal and hygrothermal curing, *MATEC Web Conf.* 10 (2014) 02004, <https://doi.org/10.1051/mateconf/20141002004>.
- [67] T. Kulovaná, E. Vejmelková, M. Keppert, P. Rovnaníková, Z. Keršner, R. Černý, Mechanical, durability and hygrothermal properties of concrete produced using Portland cement-ceramic powder blends, *Struct. Concr.* 17 (1) (2016) 105–115, <https://doi.org/10.1002/suco.201500029>.
- [68] A. Mateos, J. Harvey, J. Bolander, R. Wu, J. Paniagua, F. Paniagua, Field evaluation of the impact of environmental conditions on concrete moisture-related shrinkage and coefficient of thermal expansion, *Constr. Build. Mater.* 225 (2019) 348–357, <https://doi.org/10.1016/j.conbuildmat.2019.07.131>.